J. Fluid Mech. (1993), *vol.* 247, *pp.* 661–688

Transonic nozzle flow of dense gases

By A. KLUWICK

Institut für Strömungslehre und Wärmeübertragung, Technische Universität Wien, A-1040 Wien, Austria

(Received 27 February 1992 and in revised form 4 August 1992)

The paper deals with the flow properties of dense gases in the throat area of slender nozzles. Starting from the Navier–Stokes equations supplemented with realistic equations of state for gases which have relatively large specific heats a novel form of the viscous transonic small-perturbation equation is derived. Evaluation of the inviscid limit of this equation shows that three sonic points rather than a single sonic point may occur during isentropic expansion of such media, in contrast to the case of perfect gases. As a consequence, a shock-free transition from subsonic to supersonic speeds cannot, in general, be achieved by means of a conventional converging–diverging nozzle. Nozzles leading to shock-free flow fields must have an unusual shape consisting of two throats and an intervening antithroat. Additional new results include the computation of the internal thermoviscous structure of weak shock waves and a phenomenon referred to as impending shock splitting. Finally, the relevance of these results to the description of external transonic flows is discussed briefly.

1. Introduction

The study of materials which exhibit new and unconventional properties is of central importance for the development of advanced and refined technologies in many fields of engineering science. In this connection there has been a rapidly growing interest in real fluid effects on steady and unsteady flows in the past few years. Here the notation 'real' is not meant simply to imply the incorporation of dissipative mechanisms such as internal friction, heat conduction, etc. which are neglected in studies dealing with ideal fluids. Rather, it signals the occurrence of new effects which are present even in situations where dissipation plays an insignificant role. A prominent example is provided by dense gases which have the distinguishing feature that the so-called fundamental derivative

$$\Gamma = \frac{1}{\tilde{a}} \frac{\partial(\tilde{\rho}\tilde{a})}{\partial \tilde{\rho}}\bigg|_{\tilde{s}}$$

is negative over a finite range of temperatures and pressures, figure 1. Here $\tilde{a} = (\partial\tilde{p}/\partial\tilde{\rho})_{\tilde{s}}^{\frac{1}{2}}$ is the local speed of sound and $\tilde{p}$, $\tilde{\rho}$ and $\tilde{s}$ are the pressure, the density and the entropy.

1.1. *Bethe–Zel'dovich–Thompson (BZT) fluids*

If the isentropes in the $\tilde{p}, 1/\tilde{\rho}$ diagram are curved up then $\Gamma > 0$ and the properties of steady as well as unsteady flows qualitatively resemble those of perfect gases having $\Gamma = \frac{1}{2}(\gamma+1)$ where γ denotes the ratio of the specific heats. It has already been shown, however, by Bethe (1942) and independently by Zel'dovich (1946) that Van der Waals gases may exhibit regions where the isentropes are curved down, e.g. regions where $\Gamma < 0$, provided the specific heats take on sufficiently large values.

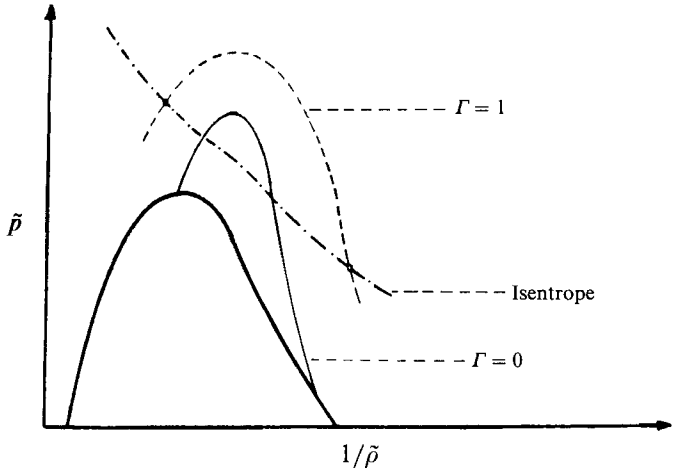

FIGURE 1. Schematic of $(\tilde{p}, 1/\tilde{\rho})$-diagram showing regions of $\Gamma > 0$ and $\Gamma < 0$.

More recent studies based on relatively sophisticated equations of state including that of Martin & Hou (1955) are due to Thompson and coworkers (Thompson 1971; Thompson & Lambrakis 1973) who gave specific examples of fluids having $\Gamma < 0$ which include hydrocarbons and fluorocarbons of moderate complexity. Because of the significance of each of these studies we refer to such fluids as Bethe–Zel'dovich–Thompson (BZT) fluids. For a thorough discussion of the Martin–Hou equation in the context of the fundamental derivative the reader is referred to Lambrakis & Thompson (1972), Thompson & Lambrakis (1973) and Cramer (1989).

Detailed investigations performed over the past ten years (as documented for example in the review articles by Cramer 1991*a*, Kluwick 1991) have revealed a number of phenomena which may occur in flows of BZT fluids but have no counterpart in the classical theory of gases with $\Gamma > 0$. Examples include expansion shocks, the partial disintegration of both compression and expansion shocks, shock splitting and sonic shocks. By sonic shock we mean a shock having a speed which coincides with the convected sound speed just upstream or downstream of the shock.

Recent studies dealing with the properties of dense gases indicate that they may indeed represent preferable working fluids in many engineering applications as for example in organic Rankine cycles. In this case as well as in other cases of practical interest it is necessary to accelerate the medium to high subsonic or even supersonic speeds. How this can be achieved in variable-area ducts is the topic of the present paper.

1.2. *Isentropic expansion of BZT fluids*

As a starting point it is useful to consider the variation of the Mach number M along isentropes which cross the negative-Γ region as the density decreases starting from an arbitrary stagnation value. Differentiation of the energy equation for steady flows,

$$\tilde{h} + \tfrac{1}{2}\tilde{a}^2 M^2 = \text{const.}, \tag{1.1}$$

where $\tilde{h}$ denotes the enthalpy, with respect to $\tilde{\rho}$ leads to the relationship

$$\left.\frac{\mathrm{d}M}{\mathrm{d}\tilde{\rho}}\right|_s = \frac{M}{\tilde{\rho}} J(\tilde{\rho}, M), \quad J = 1 - \Gamma - \frac{1}{M^2} \tag{1.2}$$

first derived by Thompson (1971). According to this result the Mach number increases with decreasing density if $\Gamma > 1$. For this reason the line $\Gamma = 1$ is included

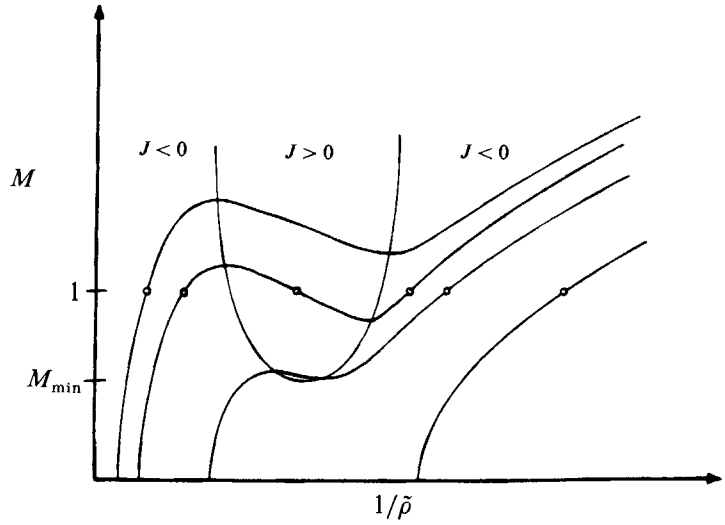

FIGURE 2. Mach number variation during isentropic expansion.

in figure 1 in addition to the so-called transition line $\Gamma = 0$. If the fluid, therefore, expands isentropically starting from stagnation conditions to the right of the line $\Gamma = 1$ the quantity J is always negative and the Mach number increases monotonically with decreasing values of $\tilde{\rho}$ just as in the case of a perfect gas. However, as the value of the stagnation density increases, the corresponding M versus $\tilde{\rho}$ curves will eventually penetrate into the region where the quantity J is positive, figure 2. Inside this region M is seen to decrease during the expansion process. Even so, however, sonic conditions $M = 1$ are reached, in general, only once: either before the isentrope enters the $J > 0$ region or after this region has been left. In the vicinity of the critical point $M = 1$ the Mach number then varies linearly with $\tilde{\rho}$ and by analogy with the perfect gas case one concludes that a full supersonic expansion can be attained by means of a classical converging–diverging Laval nozzle.

In addition, there exist also exceptional cases where the M versus $1/\tilde{\rho}$ curves exhibit three sonic points rather than a single one. Flows of this type have not been studied in detail so far. However, some insight into the behaviour of such flows can be gained if it is assumed that the thermodynamic state corresponding to critical flow conditions $M = 1$ is characterized by a point located in the vicinity of or at the transition line $\Gamma = 0$. Obviously, two different cases have to be distinguished.

In the first case sonic flow conditions are reached near one of the high- or low-pressure zeros of Γ: $\Gamma = 0$, $\partial\Gamma/\partial\tilde{\rho}|_{\tilde{s}} \neq 0$. One then finds that two of the three sonic points lie in the neighbourhood of the $J = 0$ curve. An analysis of transonic nozzle flow based on this assumption has recently been carried out by Chandrasekar & Prasad (1991).

In the second case to be investigated in the present paper sonic flow conditions are reached in the vicinity of the point where the equilibrium isentrope touches the transition line: $\Gamma = 0$, $\partial\Gamma/\partial\tilde{\rho}|_{\tilde{s}} = 0$. As a consequence, the value of the Mach number M_{min} characterizing the minimum of the $J > 0$ region differs only slightly from 1 and all three sonic points which occur during isentropic expansion almost collapse onto the curve $J = 0$.

Both situations outlined so far may – at first sight – appear somewhat artificial.

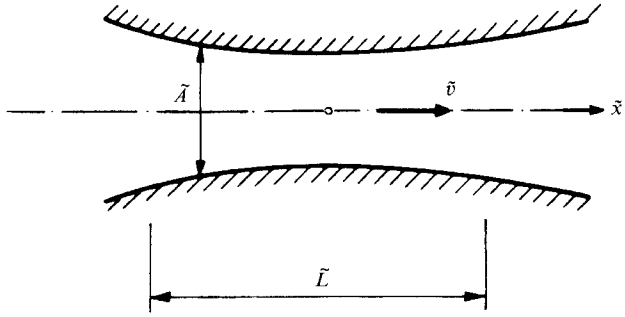

FIGURE 3. Sketch showing nozzle geometry and notation.

From the viewpoint of possible practical applications the opposite should be true, however. In order to utilize the potential advantages of BZT fluids, e.g. the smallness of the entropy losses across shocks, the thermodynamic state of the working fluid should be close to a state having $\Gamma = 0$ and if possible also $\partial\Gamma/\partial\tilde{\rho}|_{\tilde{s}} = 0$. Furthermore, apart from being of interest in its own right the study of this latter case is expected to give a qualitatively good picture of the general case that the M versus $1/\tilde{\rho}$ curve exhibits three sonic points.

2. Problem formulation

The problem considered and the notation used are shown in figure 3. We investigate the flow of a BZT fluid through a variable-area duct or nozzle. The consideration will be restricted to the throat region of the nozzle where the local Mach number M differs only slightly form the critical value $M = 1$. Furthermore, it will be assumed that the cross-section area $\tilde{A}$ changes sufficiently slowly with distance $\tilde{x}$ so that the variation of the various flow quantities in the direction normal to the nozzle axis is negligibly small. As a consequence, the appropriate form of the governing equations is given by the one-dimensional version of the Navier–Stokes equations. Owing to the transonic nature of the flow it is natural to non-dimensionalize these equations such that

$$\left.\begin{gathered}\tilde{x} = \tilde{L}x, \quad \tilde{A} = \tilde{A}_0 A, \quad \tilde{v} = \tilde{a}_0 v, \quad \tilde{\rho} = \tilde{\rho}_0 \rho, \quad \tilde{s} = \tilde{c}_{v0} s, \quad \tilde{p} = \tilde{\rho}_0 \tilde{a}_0^2 p, \\ \tilde{T} = \tilde{T}_0 T, \quad \tilde{h} = \tilde{a}_0^2 h, \quad \tilde{a} = \tilde{a}_0 a, \quad \tilde{k} = \tilde{k}_0 k, \quad \tilde{\lambda} = \tilde{\lambda}_0 \lambda, \quad \tilde{\mu} = \tilde{\mu}_0 \mu \\ \tilde{c}_p = \tilde{c}_{p0} c_p, \quad \tilde{c}_v = \tilde{c}_{v0} c_v,\end{gathered}\right\} \tag{2.1}$$

where $\tilde{v}$, $\tilde{\rho}$, $\tilde{s}$, $\tilde{p}$, $\tilde{T}$, $\tilde{h}$, $\tilde{k}$, $\tilde{\lambda}$, $\tilde{\mu}$, $\tilde{c}_p$ and $\tilde{c}_v$ denote, respectively, the velocity, density, entropy, pressure, temperature, enthalpy, thermal conductivity, first and second viscosities, specific heats at constant pressure and volume and the subscript 0 denotes quantities evaluated at the sonic reference state. $\tilde{L}$ and $\tilde{A}_0$ characterize the length and the cross-sectional area of the throat region and $\tilde{a} = (\partial\tilde{p}/\partial\tilde{\rho}|_{\tilde{s}})^{\frac{1}{2}}$ is the speed of sound. The continuity equation, momentum equation and energy equation then read

$$\frac{1}{A}\frac{\mathrm{d}A}{\mathrm{d}x} + \frac{1}{\rho}\frac{\mathrm{d}\rho}{\mathrm{d}x} + \frac{1}{v}\frac{\mathrm{d}v}{\mathrm{d}x} = 0, \tag{2.2}$$

$$\rho v \frac{\mathrm{d}v}{\mathrm{d}x} = -\frac{\mathrm{d}p}{\mathrm{d}x} + \frac{1}{Re}\frac{\mathrm{d}}{\mathrm{d}x}\left\{\left(2\mu + \frac{\tilde{\lambda}_0}{\tilde{\mu}_0}\lambda\right)\frac{\mathrm{d}v}{\mathrm{d}x}\right\}, \tag{2.3}$$

$$\rho T v \frac{\mathrm{d}s}{\mathrm{d}x} = \frac{1}{Re}\left\{Ec\left(2\mu + \frac{\tilde{\lambda}_0}{\tilde{\mu}_0}\lambda\right)\left(\frac{\mathrm{d}v}{\mathrm{d}x}\right)^2 + \frac{\gamma_0}{Pr}\frac{\mathrm{d}}{\mathrm{d}x}\left(k\frac{\mathrm{d}T}{\mathrm{d}x}\right)\right\}. \tag{2.4}$$

Here $\gamma_0 = \tilde{c}_{p0}/\tilde{c}_{v0}$ is the ratio of the specific heats and

$$Re = \tilde{a}_0 \tilde{\rho}_0 \tilde{L}/\tilde{\mu}_0, \quad Pr = \tilde{\mu}_0 \tilde{c}_{p0}/\tilde{k}_0, \quad Ec = \tilde{a}_0^2/(\tilde{c}_{v0}\tilde{T}_0) \tag{2.5}$$

denote the Reynolds, Prandtl and Eckert numbers.

In the inviscid limit $\tilde{k}$, $\tilde{\lambda}$, $\tilde{\mu} = 0$, i.e. $Re^{-1} = 0$, equations (2.2), (2.3) and (2.4) have to be supplemented with the shock jump conditions

$$[\rho v] = 0, \tag{2.6}$$

$$v_a v_b [\rho] = [p], \tag{2.7}$$

$$2\rho_a \rho_b [h] = (\rho_a + \rho_b)[p], \tag{2.8}$$

$$[s] \geqslant 0, \tag{2.9}$$

where the brackets denote jumps, i.e. $[U] = U_a - U_b$, and the subscripts a and b refer to conditions after and before the shock.

3. Viscous small-perturbation equation

In this section we derive a single equation which governs the density distribution in the transonic region of the nozzle. To this end it is convenient to eliminate the pressure gradient in the momentum equation using the relationship

$$\mathrm{d}p = a^2 \mathrm{d}\rho + \frac{\rho a^2 \tilde{\beta} \tilde{T}}{c_p \gamma_0} \mathrm{d}s, \tag{3.1}$$

where $\tilde{\beta}$ is the coefficient of thermal expansion

$$\tilde{\beta} = -\frac{1}{\tilde{\rho}} \frac{\partial \tilde{\rho}}{\partial \tilde{T}}\bigg|_{\tilde{p}} \tag{3.2}$$

which is assumed to be positive, $\tilde{\beta} > 0$.

Combining (2.2), (2.3) and (3.1) one then obtains

$$\frac{\rho M^2 a^2}{A} \frac{\mathrm{d}A}{\mathrm{d}x} + a^2(M^2 - 1) \frac{\mathrm{d}\rho}{\mathrm{d}x} - \frac{\rho a^2 \tilde{\beta} \tilde{T}}{c_p \gamma_0} \frac{\mathrm{d}s}{\mathrm{d}x} + \frac{1}{Re} \frac{\mathrm{d}}{\mathrm{d}x}\left[\left(2\mu + \frac{\tilde{\lambda}_0}{\tilde{\mu}_0}\lambda\right)\frac{\mathrm{d}v}{\mathrm{d}x}\right] = 0. \tag{3.3}$$

3.1. *Small-disturbance approximations*

Since considerations will be limited to the neighbourhood of the throat area of the nozzle where $|M-1| \ll 1$ we expect $\mathrm{d}A/\mathrm{d}x$ to be much smaller than $\mathrm{d}\rho/\mathrm{d}x, \mathrm{d}v/\mathrm{d}x$. Evaluation of the continuity equation (2.2) therefore yields the usual transonic approximation

$$\mathrm{d}v/\mathrm{d}x \sim -\mathrm{d}\rho/\mathrm{d}x. \tag{3.4}$$

Here we are concerned with weakly dissipative flows, i.e. $Re \gg 1$. In this limit, the energy equation (2.4) reduces to

$$T \frac{\mathrm{d}s}{\mathrm{d}x} \sim \frac{1}{Re} \frac{\gamma_0}{Pr} \frac{\mathrm{d}^2 T}{\mathrm{d}x^2} + \ldots. \tag{3.5}$$

As a result, entropy disturbances are small and the constitutive relationship $T = T(\rho, s)$ can be approximated by

$$\frac{\mathrm{d}T}{\mathrm{d}x} \sim \frac{\tilde{\beta}_0 \tilde{a}_0^2}{\tilde{c}_{p0}} \frac{\mathrm{d}\rho}{\mathrm{d}x} + \ldots. \tag{3.6}$$

To leading order, (3.3) thus assumes the form

$$(M-1)\frac{\mathrm{d}\rho}{\mathrm{d}x}+\frac{1}{2}\frac{\mathrm{d}A}{\mathrm{d}x}=\frac{1}{2Re}\left[\frac{\tilde{\beta}_0^2\tilde{T}_0\tilde{\alpha}_0^2}{\tilde{c}_{p0}Pr}+\left(2+\frac{\tilde{\lambda}_0}{\tilde{\mu}_0}\right)\right]\frac{\mathrm{d}^2\rho}{\mathrm{d}x^2}. \tag{3.7}$$

3.2. *Mach number–density relationship*

As shown in Thompson (1971), Cramer (1991*b*) the variation of M with ρ under isentropic flow conditions is given by

$$\left.\frac{\mathrm{d}M}{\mathrm{d}\rho}\right|_s=\frac{M}{\rho}\left(1-\Gamma-\frac{1}{M^2}\right). \tag{3.8}$$

Taylor series expansion of M about the basic state $M=1$ assuming that the fundamental derivative is expressed in terms of ρ and s: $\Gamma=\Gamma(\rho,s)$, then yields

$$\begin{aligned}M-1=&-\Gamma_0(\rho-1)+\tfrac{1}{2}(\Gamma_0^2-\Gamma_0-\Lambda_0)(\rho-1)^2\\&+\tfrac{1}{6}(3\Gamma_0^3-3\Gamma_0^2+14\Gamma_0-4\Lambda_0+5\Gamma_0\Lambda_0-N_0)(\rho-1)^3+o((\rho-1)^3),\end{aligned} \tag{3.9}$$

with

$$\left.\begin{aligned}\Lambda&=(\partial\Gamma/\partial\rho)(\rho,s),\\N&=(\partial^2\Gamma/\partial\rho^2)(\rho,s).\end{aligned}\right\} \tag{3.10}$$

As before, the subscript 0 is used to denote quantities evaluated in the reference state $\rho=1$, $s=s_0$.

Let $\epsilon\ll 1$ be a measure of the small density disturbances inside the throat area, i.e.

$$\rho=1+\epsilon\rho_1+o(\epsilon). \tag{3.11}$$

In the case considered here the sonic state of the fluid is reached in the vicinity of the point where the isentrope is tangent to the transition line $\Gamma=0$. Γ, Λ and N therefore satisfy the order of magnitude relationships

$$\left.\begin{aligned}\Gamma&=\epsilon^2\hat{\Gamma},&\hat{\Gamma}&=0(1),\\\Lambda&=\epsilon\hat{\Lambda},&\hat{\Lambda}&=0(1),\\N&=\hat{N},&\hat{N}&=0(1).\end{aligned}\right\} \tag{3.12}$$

Substituting (3.11), (3.12), into (3.9) one obtains

$$M-1=-\epsilon^3[\hat{\Gamma}_0\rho_1+\tfrac{1}{2}\hat{\Lambda}_0\rho_1^2+\tfrac{1}{6}\hat{N}_0\rho_1^3]+o(\epsilon^3). \tag{3.13}$$

3.3. *Modified viscous transonic small-perturbation equation*

If the effects of the slowly changing area of cross-section and weak dissipation are to be retained in (3.7) we have to require

$$A=1+\epsilon^4A_1+o(\epsilon^4),\quad Re=\sigma\epsilon^{-3},\quad \sigma=0(1). \tag{3.14}$$

In this distinguished limit, combination of (3.7), (3.11) and (3.13) yields the modified viscous transonic small-perturbation equation

$$-(\hat{\Gamma}_0\rho_1+\tfrac{1}{2}\hat{\Lambda}_0\rho_1^2+\tfrac{1}{6}\hat{N}_0\rho_1^3)\frac{\mathrm{d}\rho_1}{\mathrm{d}x}+\frac{1}{2}\frac{\mathrm{d}A_1}{\mathrm{d}x}=\tfrac{1}{2}\delta_0\frac{\mathrm{d}^2\rho_1}{\mathrm{d}x^2}. \tag{3.15}$$

The quantity δ_0

$$\delta_0 = \frac{\bar{\delta}_0}{\epsilon^3}, \quad \bar{\delta}_0 = \frac{1}{Re}\left[\frac{\tilde{\lambda}_0}{\tilde{\mu}_0} + 2 + \frac{\tilde{\beta}_0^2 \tilde{T}_0 \tilde{a}_0^2}{\tilde{c}_{p0} Pr}\right] \tag{3.16}$$

is essentially the acoustic diffusivity of a general fluid, e.g. Cramer & Kluwick (1984). It is of interest to note the differences between the scalings as expressed by (3.14) and the classical results for perfect gases: $A-1 = O(\epsilon^2)$, $Re = O(\epsilon^{-1})$. These are, of course, an immediate consequence of the basic assumption adopted here that the fundamental derivative is small rather than of order one, which results in a much weaker nonlinearity.

Introducing the expansions

$$\left.\begin{aligned} v &= 1 + \epsilon v_1 + o(\epsilon), \quad T = 1 + \epsilon T_1 + o(\epsilon), \\ p &= p_0 + \epsilon p_1 + o(\epsilon), \quad s = s_0 + \epsilon^4 s_1 + o(\epsilon^4) \end{aligned}\right\} \tag{3.17}$$

similar to (3.11), evaluation of (3.1), (3.4), (3.5) and (3.6) yields

$$v_1 = -\rho_1, \quad T_1 = \frac{\tilde{\beta}_0 \tilde{a}_0^2}{\tilde{c}_{p0}} \rho_1, \quad p_1 = \rho_1, \quad s_1 = \frac{\tilde{\beta}_0 \tilde{a}_0^2}{\sigma Pr \tilde{c}_{v0}} \frac{\mathrm{d}\rho_1}{\mathrm{d}x}. \tag{3.18}$$

It is convenient to write (3.15) in the equivalent form

$$j_1 + A_1 = Q = \text{const.}, \tag{3.19}$$

where

$$j_1 = -\hat{\Gamma}_0 \rho_1^2 - \tfrac{1}{3}\hat{A}_0 \rho_1^3 - \tfrac{1}{12}\hat{N}_0 \rho_1^4 - \frac{\delta_0 \mathrm{d}\rho_1}{\mathrm{d}x} \tag{3.20}$$

is the density of the perturbation mass flux. Here the first three terms describe the variation of j_1 with ρ_1 under isentropic flow conditions while the last term accounts for the entropy changes caused by internal friction and heat conduction.

4. Inviscid flow

4.1. *The* (j_1, ρ_1)*-diagram*

In the limit $Re \to \infty$, i.e. $\delta_0 \to 0$, equation (3.20) reduces to an algebraic relationship between the perturbation mass flux and the density disturbances

$$j_1 = -\hat{\Gamma}_0 \rho_1^2 - \tfrac{1}{3}\hat{A}_0 \rho_1^3 - \tfrac{1}{12}\hat{N}_0 \rho_1^4. \tag{4.1}$$

Using this result, (3.13) which determines the Mach number variation during isentropic expansion or compression can be written in the form

$$(M-1)/\epsilon^3 = \tfrac{1}{2}\mathrm{d}j_1/d\rho_1. \tag{4.2}$$

Furthermore, Taylor series expansion about the reference state leads to the following leading-order expressions for the scaled local values of the fundamental derivative and its derivative with respect to ρ:

$$\hat{\Gamma} = -\tfrac{1}{2}\mathrm{d}^2 j_1/\mathrm{d}\rho_1^2, \quad \hat{A} = -\tfrac{1}{2}\mathrm{d}^3 j_1/\mathrm{d}\rho_1^3. \tag{4.3}$$

$M-1$ and Γ, therefore, change sign at values of ρ_1 corresponding to stationary and inflexion points of the j_1 versus ρ_1 diagram, respectively. A typical $j_1(\rho_1)$ curve is sketched in figure 4 for a reference state having positive values of both $\hat{\Gamma}_0$ and $\hat{A}_0$.

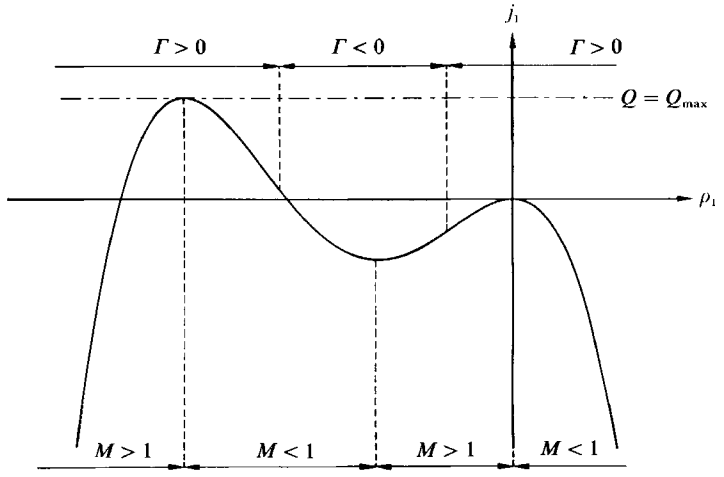

FIGURE 4. (j_1, ρ_1)-diagram corresponding to a reference state with $\hat{\Gamma}_0 > 0$, $\hat{\Lambda}_0 > 0$.

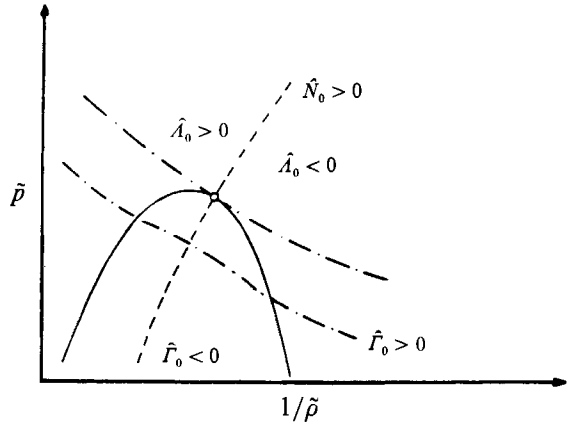

FIGURE 5. Regions of $\hat{\Gamma}_0 \gtrless 0$ and $\hat{\Lambda}_0 \gtrless 0$ in the $(\tilde{p}, 1/\tilde{\rho})$-plane: ——, transition line $\Gamma = 0$; - - - - -, line $\Lambda = 0$; –·–·–, isentropes.

Regions of the $(\tilde{p}, 1/\tilde{\rho})$-plane where $\hat{\Gamma}_0$ and $\hat{\Lambda}_0$ assume positive and negative values, respectively, are depicted schematically in figure 5. Furthermore, figure 6 indicates the variation of the $j_1(\rho_1)$-diagram as the reference state crosses the negative-Γ region along an isentrope starting at a point near one of the high-pressure zeros of Γ. If $\hat{\Gamma}_0 \gg \hat{\Lambda}_0^2/\hat{N}_0$ the plots qualitatively resemble the perfect gas result, i.e. the j_1 versus ρ_1 diagram exhibits a single maximum at $\rho_1 = \rho_1^* = 0$ corresponding to the single sonic state which occurs during isentropic expansion. If $\hat{\Gamma}_0 < 3\hat{\Lambda}_0^2/(8\hat{N}_0)$, however, sonic conditions are reached in addition at

$$\rho_1 = \rho_1^* = -\frac{3\hat{\Lambda}_0}{2\hat{N}_0}\left[1 \pm \left(1 - \frac{8\hat{\Gamma}_0\hat{N}_0}{3\hat{\Lambda}_0^2}\right)^{\frac{1}{2}}\right] \tag{4.4}$$

and, as a result, the associated (j_1, ρ_1)-plots show two maxima and one minimum. The two values of ρ_1^* given by (4.4) correspond, respectively, to a sonic state inside the $\Gamma < 0$ region and a sonic state in the vicinity of the low-pressure branch of the transition line $\Gamma = 0$ having $\Gamma > 0$. Consequently, not all the curves included in figure 6 correspond to cases which are physically independent. In fact, if the reference state is identified with the sonic state which occurs first during isentropic expansion

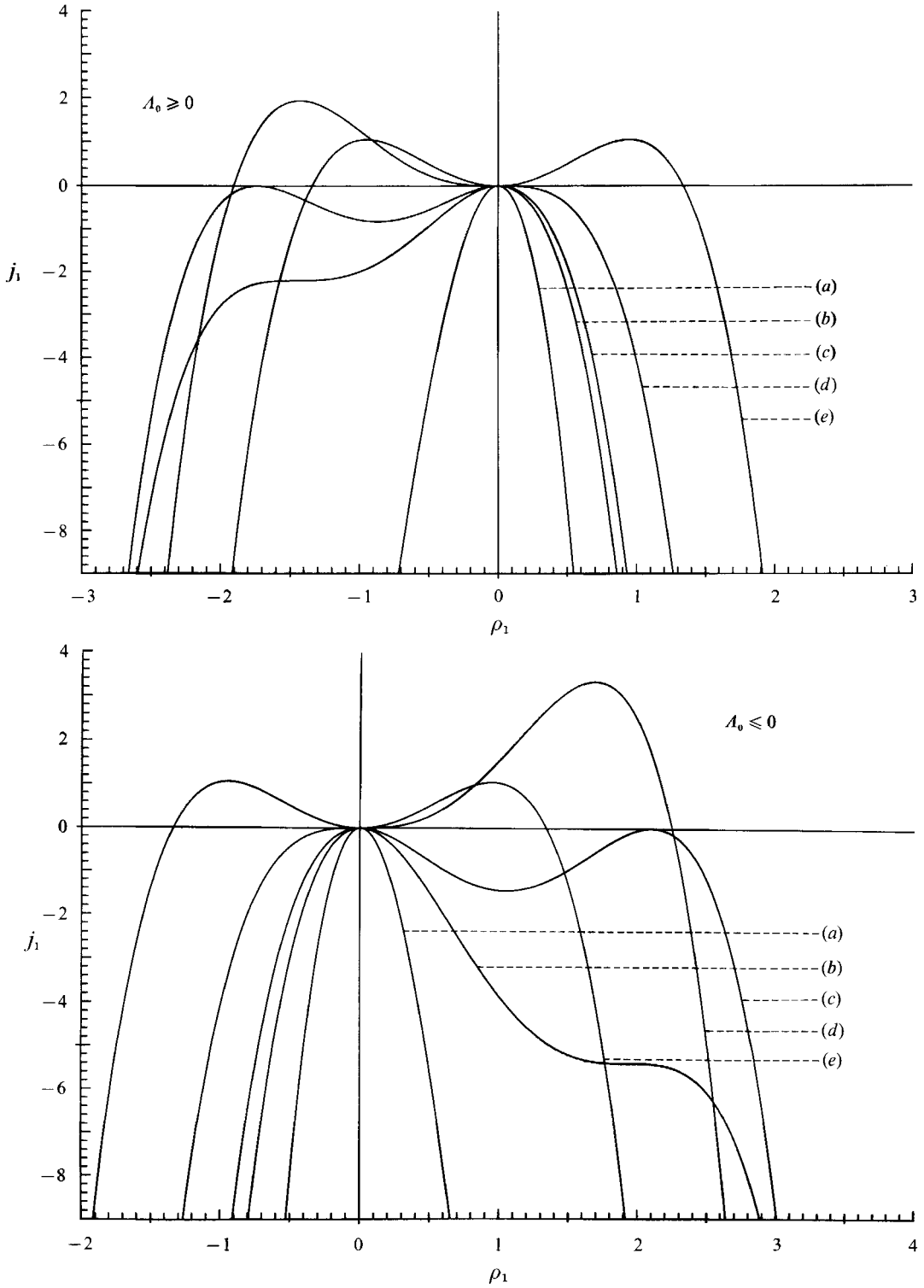

FIGURE 6. Variation of the (j_1, ρ_1)-diagram as the reference state varies along an isentrope which passes through the negative-Γ region: (*a*) $\hat{\Gamma}_0 \gg 1$, (*b*) $\hat{\Gamma}_0 = 3\hat{\Lambda}_0^2/8\hat{N}_0$, (*c*) $\hat{\Gamma}_0 = \hat{\Lambda}_0^2/3\hat{N}_0$, (*d*) $\hat{\Gamma}_0 = 0$, (*e*) $\hat{\Lambda}_0 = 0$.

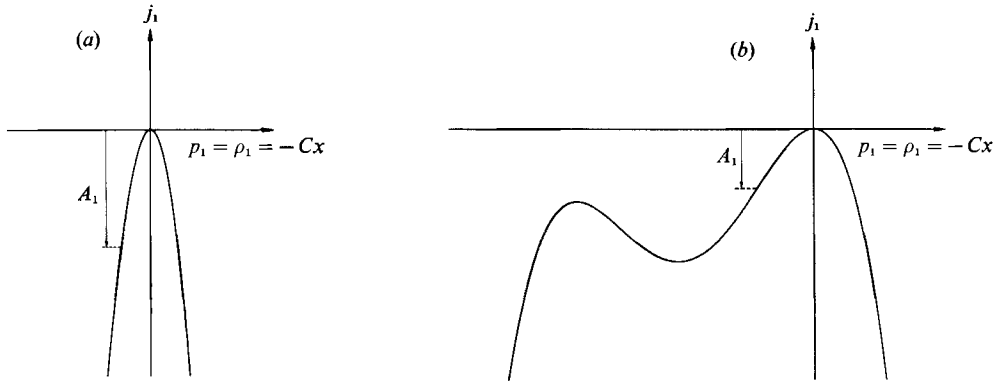

FIGURE 7. Subsonic–supersonic expansion of BZT fluids: nozzle shape leading to a linear density distribution. (*a*) $\hat{\Gamma}_0 > 3\hat{A}_0^2/(8\hat{N}_0)$, (*b*) $\hat{\Gamma}_0 < 3\hat{A}_0^2/(8\hat{N}_0)$.

starting from stagnation conditions it suffices to investigate the parameter range $\hat{\Gamma}_0 \geqslant 0$, $\hat{A}_0 > 0$. Although other choices may be more convenient in some situations from a practical point of view the following considerations will be limited to this parameter range for brevity.

4.2. *Nozzle shapes leading to linear density/pressure distributions*

According to (3.18), (3.19) the (j_1, ρ_1)-relationship (4.1) can be used immediately to design a nozzle which yields a prescribed density (pressure, etc.) distribution or to determine the density (pressure, etc.) distribution in a nozzle of given shape. In this connection it is useful to note a simple geometrical interpretation of the linearized continuity equation (3.19): the cross-sectional A_1 corresponding to a specific value of the density ρ_1 is given by the distance between the line $j_1 = Q = \text{const.}$ and the j_1 versus ρ_1 graph.

As a first example we consider the acceleration of a BZT-fluid from subsonic to supersonic speeds imposing the linear pressure/density distribution

$$p_1 = \rho_1 = -Cx, \tag{4.5}$$

where C is a positive constant. Evaluation of (3.19) and (3.20) then gives

$$A_1 = Q_{\max} + \hat{\Gamma}_0 C^2 x^2 - \tfrac{1}{3}\hat{A}_0 C^3 x^3 + \tfrac{1}{12}\hat{N}_0 C^4 x^4. \tag{4.6}$$

Here $Q_{\max}$ denotes the value of j_1 at the maximum of the (j_1, ρ_1)-relationship, figure 4.

As in the case of a perfect gas the shape of the nozzle qualitatively resembles the shape of the (j_1, ρ_1)-graph. A linear density distribution, therefore, can be achieved by a conventional converging–diverging nozzle if $\hat{\Gamma}_0 > 3\hat{A}_0^2/(8\hat{N}_0)$. If $\hat{\Gamma}_0 < 3\hat{A}_0^2/(8\hat{N}_0)$, however, a nozzle having two throats rather than a single throat is required, figure 7. Of course, these conclusions remain unchanged if the linear density distribution (4.5) is replaced by a monotonically decreasing function.

Equations (4.1) (4.2) and (4.5) can be combined to yield the expression

$$(M-1)/\epsilon^3 = \hat{\Gamma}_0 Cx - \tfrac{1}{2}\hat{A}_0 C^2 x^2 + \tfrac{1}{6}\hat{N}_0 C^3 x^3 \tag{4.7}$$

for the Mach number variation along the nozzle axis. With the exception of the perfect gas case $\hat{A}_0 = \hat{N}_0 = 0$, a linearly/monotonical decreasing density distribution thus does not lead to a linearly/monotonical increasing Mach number distribution. In particular, $M = 1$ in both throats and the intervening antithroat. This is in

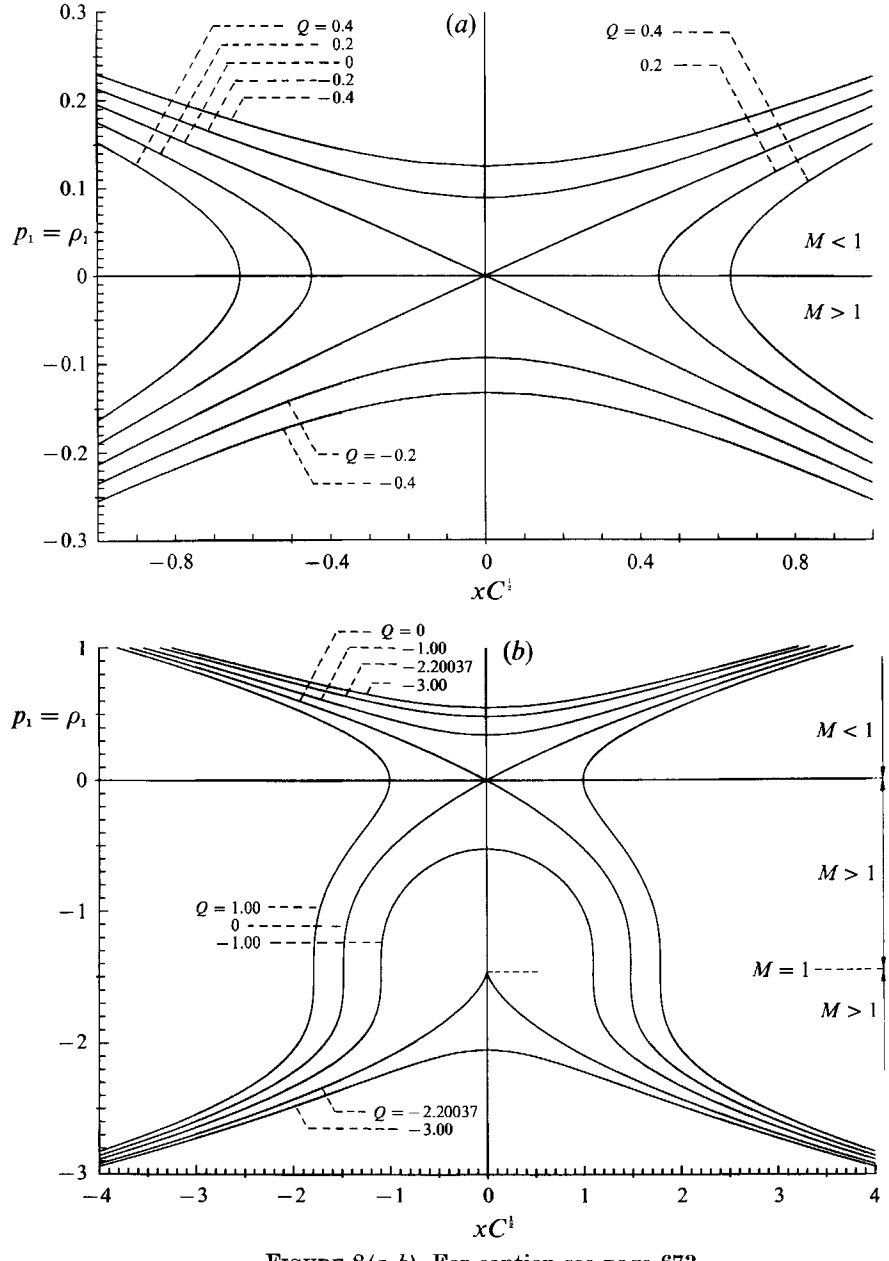

FIGURE 8(*a*, *b*). For caption see page 673.

agreement with the result first derived by Thompson (1971) that a nozzle with an antithroat is needed to achieve the transition of a negative-Γ fluid from subsonic to supersonic flow.

4.3. *Density/pressure distributions in converging–diverging nozzles*

Following this brief discussion of shock-free accelerating flows let us discuss the flow through a conventional converging–diverging nozzle in more detail. Specifically, it will be assumed that the shape of the nozzle is given by

$$A_1 = Cx^2, \quad C > 0. \tag{4.8}$$

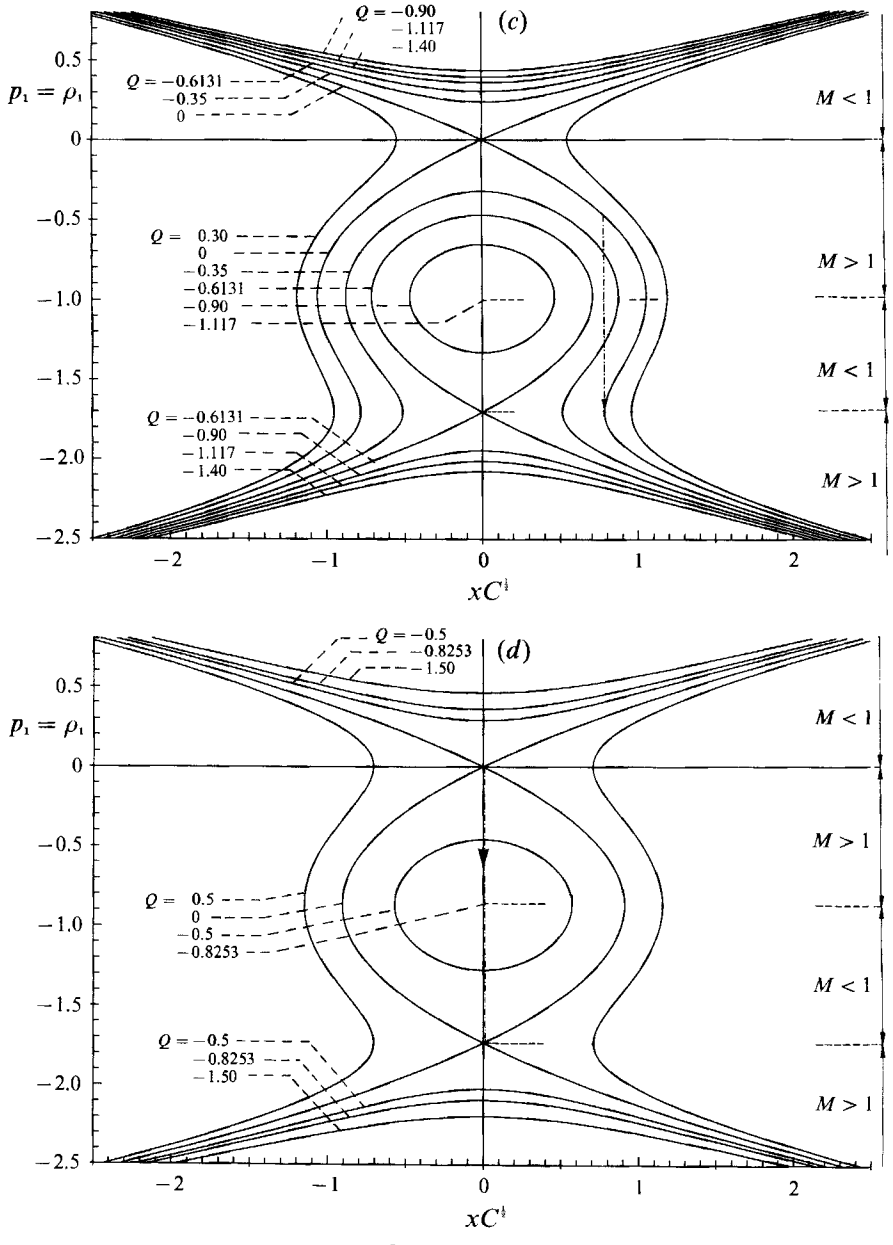

FIGURE 8(*c*, *d*). For caption see facing page.

Qualitatively similar results, however, hold for other nozzle shapes and can indeed be extracted quite simply from the results based on (4.8) taking into account that there exists a unique relationship between ρ_1 and A_1 once the value Q of the perturbation mass flux has been specified: $\rho_1 = \rho_1(A_1; Q)$.

Density contours corresponding to various values of Q are depicted in figure 8(*a–f*). If $\hat{\Gamma}_0 > 3\hat{A}_0^2/(8\hat{N}_0)$ the $j_1(\rho_1)$-curve exhibits a single maximum and the results thus qualitatively resemble the results obtained for perfect gases, e.g. there exists a single saddle point at $\rho_1 = x = 0$ and the density distributions passing through this point describe the shock-free acceleration/deceleration of the fluid from sub-

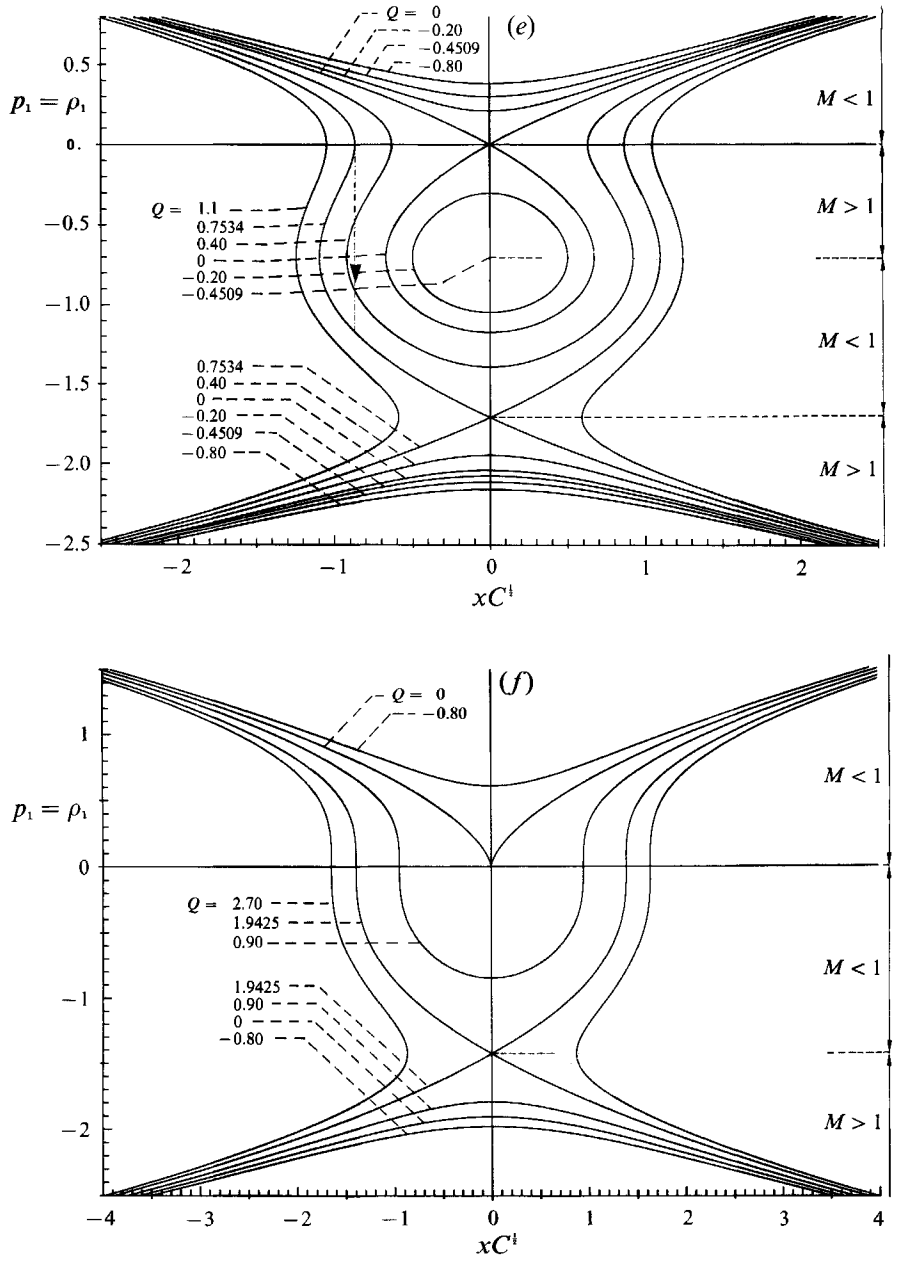

FIGURE 8. Laval nozzle: density distributions for various values of the perturbation mass flux. –·–·–·–, Shock discontinuities needed to achieve full subsonic–supersonic expansion. (*a*) $\hat{\Gamma}_0 > 3\hat{\Lambda}_0^2/(8\hat{N}_0)$: $\hat{\Gamma}_0 = 24.06$, $\hat{\Lambda}_0 = 30.96$, $\hat{N}_0 = 19.22$; (*b*) $\hat{\Gamma}_0 = 3\hat{\Lambda}_0^2/(8\hat{N}_0)$: $\hat{\Gamma}_0 = 6.26$, $\hat{\Lambda}_0 = 17.25$, $\hat{N}_0 = 17.82$; (*c*) $3\hat{\Lambda}_0^2/(8\hat{N}_0) > \hat{\Gamma}_0 > \hat{\Lambda}_0^2/(3\hat{N}_0)$: $\hat{\Gamma}_0 = 4.91$, $\hat{\Lambda}_0 = 15.80$, $\hat{N}_0 = 17.67$; (*d*) $\hat{\Gamma}_0 = \hat{\Lambda}_0^2/(3\hat{N}_0)$: $\hat{\Gamma}_0 = 4.40$, $\hat{\Lambda}_0 = 15.25$, $\hat{N}_0 = 17.61$; (*e*) $\hat{\Lambda}_0^2/(3\hat{N}_0) > \hat{\Gamma}_0 > 0$: $\hat{\Gamma}_0 = 3.48$, $\hat{\Lambda}_0 = 14.03$, $\hat{N}_0 = 17.48$; (*f*) $\hat{\Gamma}_0 = 0$: $\hat{\Gamma}_0 = 0$, $\hat{\Lambda}_0 = 8.02$, $\hat{N}_0 = 16.86$.

sonic/supersonic to supersonic/subsonic speeds. In addition there exist purely subsonic or supersonic solutions if $Q < Q_{\max} = 0$, while the density distributions cannot be continued up to and through the throat if $Q > 0$, figure 8(*a*).

If $\hat{\Gamma}_0 = 3\hat{\Lambda}_0^2/(8\hat{N}_0)$, isentropic expansion or compression of the fluid leads to sonic

conditions at $\rho_1 = 0$ and $\rho_1 = -3\hat{A}_0/2\hat{N}_0$, respectively. Since Γ vanishes for the latter value of the density perturbation all density distributions passing through this additional sonic point exhibit vertical tangents and as a result a cusp is formed at $\rho_1 = -3\hat{A}_0/2\hat{N}_0$, $x = 0$, figure 8(*b*).

A second saddle point and a centre emerge from this cusp if $\hat{\Gamma}_0$ is reduced further. Indeed, it is easily shown that each maximum/minimum of the $j_1(\rho_1)$ relationship leads to the formation of a saddle/centre located at $x = 0$, and the associated critical value of $\rho_1 = \rho_1^*$. Owing to the presence of two sonic points having $\Gamma > 0$ and an intervening sonic point having $\Gamma < 0$ all density distributions except those corresponding to purely subsonic or purely supersonic flow fold to form regions of multivaluedness. Since the density distributions passing through $x = 0$, $\rho_1 = 0$ loosely resemble the shape of a downward pointing tulip this configuration will be termed a 'tulip down' configuration, figure 8(*c*).

If $\hat{\Gamma}_0 = \hat{A}_0^2/(3\hat{N}_0)$ both maxima of the mass flux–density relationship touch the line $j_1 = 0$, figure 6. As a consequence, the density distribution corresponding to the maximum value of the perturbation mass flux $Q = Q_{\max} = 0$ passes through both saddle points, figure 8(*d*). Further reduction of $\hat{\Gamma}_0$ leads to the 'tulip up' configuration shown in figure 8(*e*). With decreasing values of $\hat{\Gamma}_0$ the centre approaches the saddle point located at $x = 0$, $\rho_1 = 0$ and a cusp is formed there in the limiting case $\hat{\Gamma}_0 = 0$, figure 8(*f*).

If ρ_1 differs only slightly from the value ρ_1^* corresponding to a sonic state $(\mathrm{d}j_1/\mathrm{d}\rho_1)_{\rho_1^*} = 0$, the j_1 versus ρ_1 relationship (4.1) can be approximated by

$$j_1 \sim j_1(\rho_1^*) - \hat{\Gamma}(\rho_1^*)\,(\rho_1 - \rho_1^*)^2, \tag{4.9}$$

which is of course just the perfect gas result where the constant value of Γ has been replaced by $\hat{\Gamma}$ evaluated at ρ_1^*. In agreement with the density distributions shown in figure 8(*a–f*) we thus infer that the minimum of the (j_1, ρ_1)-diagram leads to the occurrence of a centre at $x = 0$ while each maximum causes the formation of a saddle point

$$\left.\frac{\mathrm{d}\rho_1}{\mathrm{d}x}\right|_{\rho_1=\rho_1^*} = \pm\left(\frac{1}{2\hat{\Gamma}(\rho_1^*)}\left(\frac{\mathrm{d}^2 A_1}{\mathrm{d}x^2}\right)_{x=0}\right)^{\frac{1}{2}} \tag{4.10}$$

if $(\mathrm{d}^2A/\mathrm{d}x^2)_{x=0} > 0$ as in the case of a Laval nozzle. Furthermore, (4.10) indicates that an antithroat $(\mathrm{d}^2A/\mathrm{d}x^2)_{x=0} < 0$ is needed to accelerate the fluid continuously through a sonic state with $\Gamma < 0$ as pointed out first by Thompson (1971).

The above considerations indicate that continuous, single-valued solutions describing the acceleration of a BZT fluid from subsonic to supersonic speeds exist for $\hat{\Gamma}_0 \geqslant 3\hat{A}_0^2/(8\hat{N}_0)$ only. We therefore conclude that shocks will form inside a conventional converging–diverging nozzle if the reference state is outside this parameter range, e.g. if $\hat{\Gamma}_0 < 3\hat{A}_0^2/(8\hat{N}_0)$. To determine the correct form of the resulting flow pattern but also to complete the description of general nozzle flows we consider next the properties of weak shock discontinuities.

4.4. *Shock admissibility criteria*

Since the mass flux is continuous across a shock front, density disturbances before and after the shock satisfy the relationship

$$[j_1] = 0. \tag{4.11}$$

Corresponding values of ρ_1 in the $j_1(\rho_1)$-diagram, therefore, lie on straight lines (Rayleigh lines) which are parallel to the ρ_1-axis, figure 9.

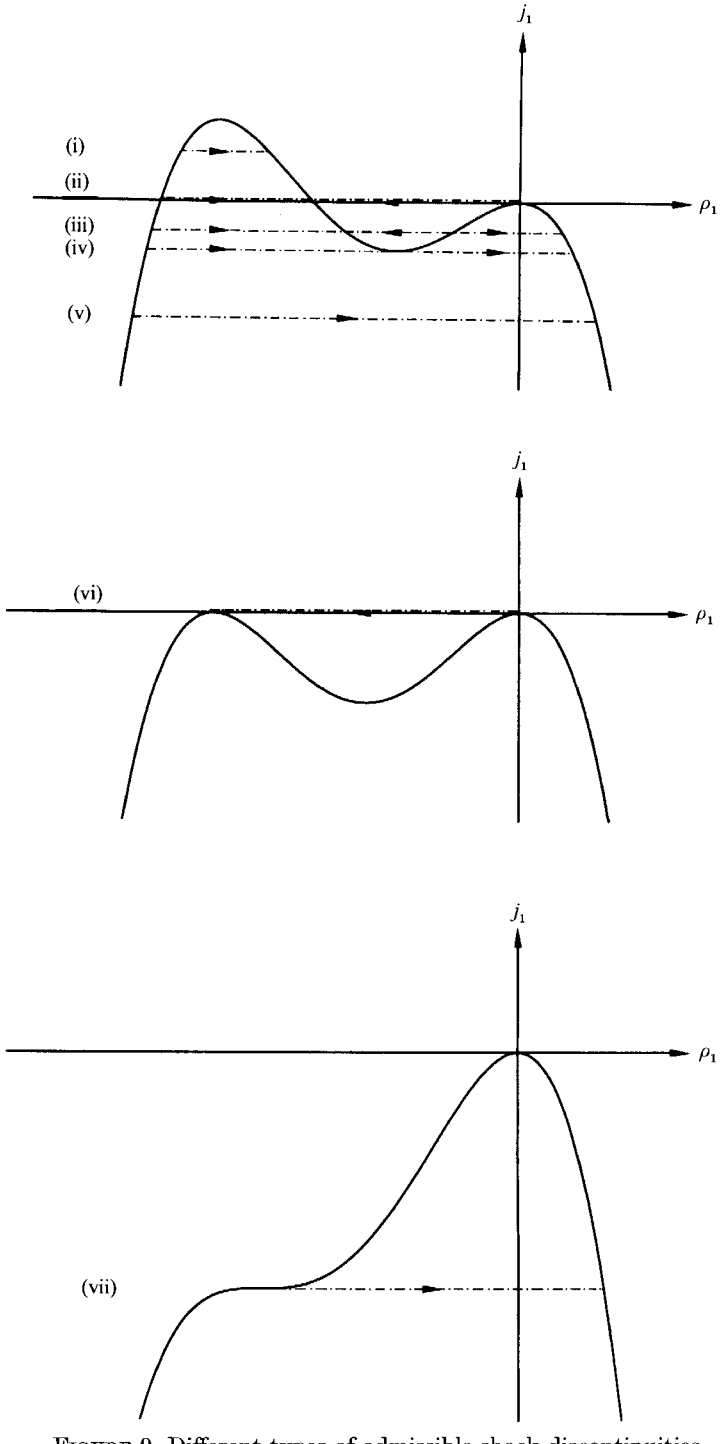

FIGURE 9. Different types of admissible shock discontinuities.

According to (2.9) the entropy s must not decrease across shock discontinuities. Substitution of the Taylor series expansions

$$h_a-h_b=\frac{\tilde{c}_{v0}\tilde{T}_0}{\tilde{a}_0^2}T_b(s_a-s_b)+V_b(p_a-p_b)+\frac{1}{2}\frac{\partial V}{\partial p}\bigg|_{s,b}(p_a-p_b)^2$$
$$+\frac{1}{6}\frac{\partial^2 V}{\partial p^2}\bigg|_{s,b}(p_a-p_b)^3+\frac{1}{24}\frac{\partial^3 V}{\partial p^3}\bigg|_{s,b}(p_a-p_b)^4+\frac{1}{120}\frac{\partial^4 V}{\partial p^4}\bigg|_{s,b}(p_a-p_b)^5+\dots,$$

$$V_a-V_b=\frac{\partial V}{\partial p}\bigg|_{s,b}(p_a-p_b)+\frac{1}{2}\frac{\partial^2 V}{\partial p^2}\bigg|_{s,b}(p_a-p_b)^2+\frac{1}{6}\frac{\partial^3 V}{\partial p^3}\bigg|_{s,b}(p_a-p_b)^3$$
$$+\frac{1}{24}\frac{\partial^4 V}{\partial p^4}\bigg|_{s,b}(p_a-p_b)^4+\dots,$$

where $V=1/\rho$ into (2.8) yields

$$\frac{\tilde{c}_{v0}\tilde{T}_0}{\tilde{a}_0^2}T_b[s]=\frac{1}{12}\frac{\partial^2 V}{\partial p^2}\bigg|_{s,b}[p]^3+\frac{1}{24}\frac{\partial^3 V}{\partial p^3}\bigg|_{s,b}[p]^4+\frac{1}{80}\frac{\partial^4 V}{\partial p^4}\bigg|_{s,b}[p]^5+\dots. \tag{4.12}$$

To the order of approximation considered here this relationship is equivalent to the expression

$$(\tilde{c}_{v0}\tilde{T}_0/\tilde{a}_0^2)[s]=\epsilon^5\{\tfrac{1}{6}\hat{\Gamma}_b[\rho_1]^3+\tfrac{1}{12}\hat{\Lambda}_b[\rho_1]^4+\tfrac{1}{40}\hat{N}_0[\rho_1]^5\}+o(\epsilon^5). \tag{4.13}$$

Here $\hat{\Gamma}_b$ and $\hat{\Lambda}_b$ characterize the scaled values of Γ and its derivative with respect to ρ immediately before the shock front. Using (4.3) these quantities are expressed in terms of the values $\hat{\Gamma}_0, \hat{\Lambda}_0$ at the reference state and the corresponding density perturbations. One obtains

$$(\tilde{c}_{v0}\tilde{T}_0/\tilde{a}_0^2)[s]=\epsilon^5\tfrac{1}{6}[\rho_1]^3\{\hat{\Gamma}_0+\tfrac{1}{2}\hat{\Lambda}_0(\rho_{1a}+\rho_{1b})$$
$$\tfrac{1}{20}\hat{N}_0(3\rho_{1a}^2+4\rho_{1a}\rho_{1b}+3\rho_{1b}^2)\}+o(\epsilon^5). \tag{4.14}$$

Evaluation of (4.2) leads to the relationship

$$[M]=-\epsilon^3[\rho_1]\{\hat{\Gamma}_0+\tfrac{1}{2}\hat{\Lambda}_0(\rho_{1a}+\rho_{1b})+\tfrac{1}{6}\hat{N}_0(\rho_{1a}^2+\rho_{1a}\rho_{1b}+\rho_{1b}^2)\}+o(\epsilon^3). \tag{4.15}$$

Equations (4.14) and (4.15) can be combined to yield the result

$$(\tilde{c}_{v0}\tilde{T}_0/\tilde{a}_0^2)[s]=-\tfrac{1}{6}\epsilon^2[\rho_1]^2[M]-\tfrac{1}{360}\epsilon^5\hat{N}_0[\rho_1]^5+o(\epsilon^5). \tag{4.16}$$

The properties of weak unsteady and steady shocks in fluids having mixed nonlinearity have been investigated by Cramer & Kluwick (1984) and by Chandrasekar & Prasad (1991) adopting the assumption that $\Gamma_0=O(\epsilon)$, $\Lambda_0=O(1)$ under reference conditions. As a consequence, the variation of Λ with the thermodynamic state could be neglected to leading order. It was found that the requirement $[s]\geqslant 0$ following from the second law of thermodynamics was too weak to rule out inadmissible shock discontinuities, e.g. shocks for which a thermoviscous profile does not exist. To eliminate inadmissible shocks, the wavespeed ordering principle expressing the requirement that shocks must lead to a supersonic–subsonic transition (including the limiting cases that sonic conditions exist either before or after the front) was imposed.

Also in the case studied here, $\Gamma_0=O(\epsilon^2)$, $\Lambda_0=O(\epsilon)$, the requirement $[s]\geqslant 0$ is found to be too weak to rule out the formation of inadmissible shocks. However, such shocks may occur even if the wave speed ordering principle is imposed. As will be

seen from the analysis of the shock structure problem discussed in the next section admissible shocks have to meet the additional condition that the Rayleigh line $j_1 =$ const. must not cut the j_1 versus ρ_1 relationship:

$$\text{shock admissibility criterion A} \begin{cases} \text{the Rayleigh line connecting the values of } \rho_1 \text{ before and after the shock must not cut intervening branches of the } (j_1, \rho_1)\text{-diagram} \\ M_b \geqslant 1 \geqslant M_a \end{cases} \tag{4.17}$$

The first condition of (4.17) is equivalent to the criterion first formulated by Oleinik (1959) in a different context. According to the second relationship of (4.17) shocks may have sonic upstream conditions $M_b = 1$ or sonic downstream conditions $M_a = 1$ (sonic shocks) but also sonic upstream and sonic downstream conditions $M_b = M_a = 1$ (double sonic shocks). In the latter case both requirements (4.17) are satisfied in a trivial manner and, therefore, they can not be used to decide whether double sonic shocks occur in the form of expansion or compression discontinuities. In order to answer this question the jump condition $[M] = 0$ holding for such shocks is inserted into (4.16) to yield

$$(\tilde{c}_{v0}\tilde{T}_0/\tilde{a}_0^2)\,[s] = -\tfrac{1}{360}\epsilon^5 \hat{N}_0 [\rho_1]^5 + o(\epsilon^5). \tag{4.18}$$

Since $\hat{N}_0$ is a positive constant we conclude that double sonic shocks can occur in the form of expansion shocks only.

The result (4.17) is useful to identify possible shock discontinuities in the (j_1, ρ_1)-plane, figure 9. To simplify the discussion of possible density distributions in a nozzle of given shape it is, however, convenient to express it in terms of ρ_1 and x. To this end we take into account that there exists a functional relationship between j_1 and x once the imposed value of the perturbation mass flux Q and the nozzle geometry characterized by the function $A_1(x)$ have been specified. As a consequence we obtain

$$\text{shock admissibility criterion B} \begin{cases} \text{the line } x = \text{const. connecting the values of } \rho_1 \text{ before and after the shock must not cut intervening branches of the density distribution} \\ M_b \geqslant 1 \geqslant M_a. \end{cases} \tag{4.19}$$

4.5. *Shock discontinuities in converging–diverging nozzles*

The admissibility criterion (4.19) can immediately be used to insert shock discontinuities into the density distributions for converging–diverging nozzles calculated earlier. Owing to the complexity of these solutions as exemplified by figure 8(*a–f*) an exhaustive discussion of all possibilities is not attempted. Rather, we restrict the considerations to a few typical examples.

As a starting point we consider the case that the medium accelerates from subsonic to supersonic speeds and discuss the changes of the flow field associated with changes of the reference state which is assumed to vary along an isentrope which crosses the negative-Γ region. If $\hat{\Gamma}_0 \geqslant 3\hat{\Lambda}_0^2/(8\hat{N}_0)$ the fluid expands in a shock-free manner similar to the perfect gas case. For smaller values of $\hat{\Gamma}_0$ the density distributions cease to be single valued and an expansion shock having sonic upstream conditions forms far

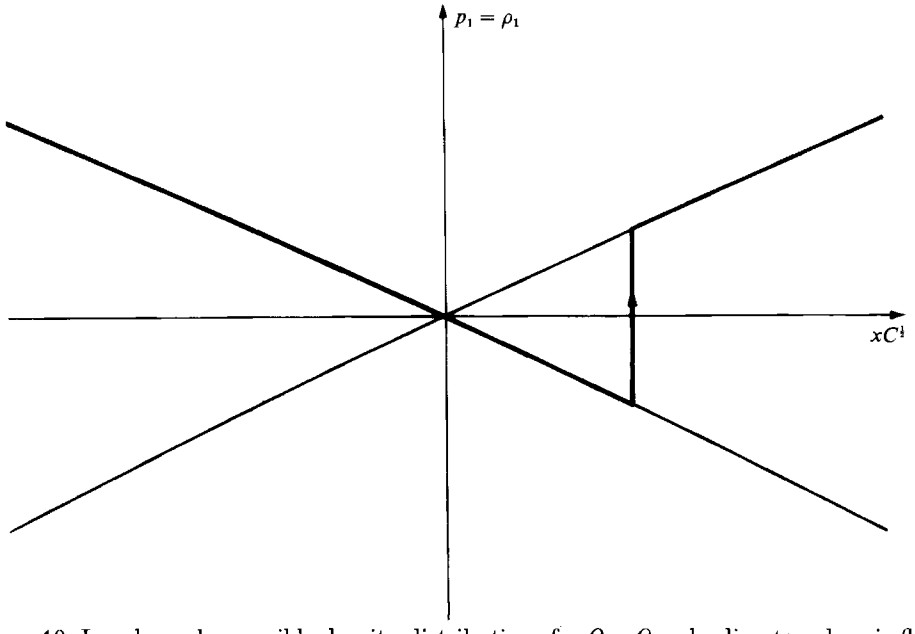

FIGURE 10. Laval nozzle: possible density distributions for $Q = Q_{max}$ leading to subsonic flow far downstream; $\hat{\Gamma}_0 = 24.06$, $\hat{A}_0 = 30.96$, $\hat{N}_0 = 19.22$.

downstream, $x \to \infty$, in the limit $\hat{\Gamma}_0 - 3\hat{A}_0^2/(8\hat{N}_0) \to 0-$. With decreasing values of $\hat{\Gamma}_0$ this shock moves upstream, figure 8(*c*). At the same time the state of the fluid downstream of the shock front approaches sonic conditions and a double sonic expansion shock is located at $x = 0$ if $\hat{\Gamma}_0 = \hat{A}_0^2/(3\hat{N}_0)$, figure 8(*d*). Further reduction of $\hat{\Gamma}_0$ causes the shock to move upstream of the throat, its position tending to $x \to \infty$ as $\hat{\Gamma}_0 \to 0$, figure 8(*e*, *f*).

As a second case we investigate flows which are accelerated from subsonic to supersonic speeds and then shocked back to a subsonic state. Similar to the theory of perfect gases, solutions of this type are found to be non-unique in the leading-order approximation considered here. If $\hat{\Gamma}_0 \geqslant 3\hat{A}_0^2/(8\hat{N}_0)$, for example, all jump discontinuities connecting the supersonic branch $Q = 0$ and the subsonic branch $Q = 0$ represent admissible compression shocks, figure 10. The local behaviour of the density distributions near $x = 0$ does not change qualitatively if $\hat{\Gamma}_0$ decreases below this value but stays in the range $3\hat{A}_0^2/(8\hat{N}_0) > \hat{\Gamma}_0 > \hat{A}_0^2/(3\hat{N}_0)$. It thus follows that solutions with sufficiently weak compression shocks qualitatively resemble those for $\hat{\Gamma}_0 \geqslant 3\hat{A}_0^2/(8\hat{N}_0)$. Solutions with stronger shocks, however, exhibit a completely different behaviour as can be seen from figure 11 which shows the variation of the flow field associated with a continuous increase of the overall density jump.

As pointed out earlier, small density jumps are achieved by single compression shocks forming just downstream of the throat, figure 11(*a*). With increasing strength the shock front moves downstream until sonic upstream conditions are reached. In order to construct solutions with larger overall density jump an additional expansion shock located upstream of this sonic compression shock has to be inserted, figure 11(*b*). As this expansion shock strengthens it is shifted to smaller values of x until it assumes a limiting position corresponding to sonic downstream conditions. By imposing a further increase of the overall density jump we are led to the three-shock configuration displayed in figure 11(*c*) which is characterized by the occurrence of a

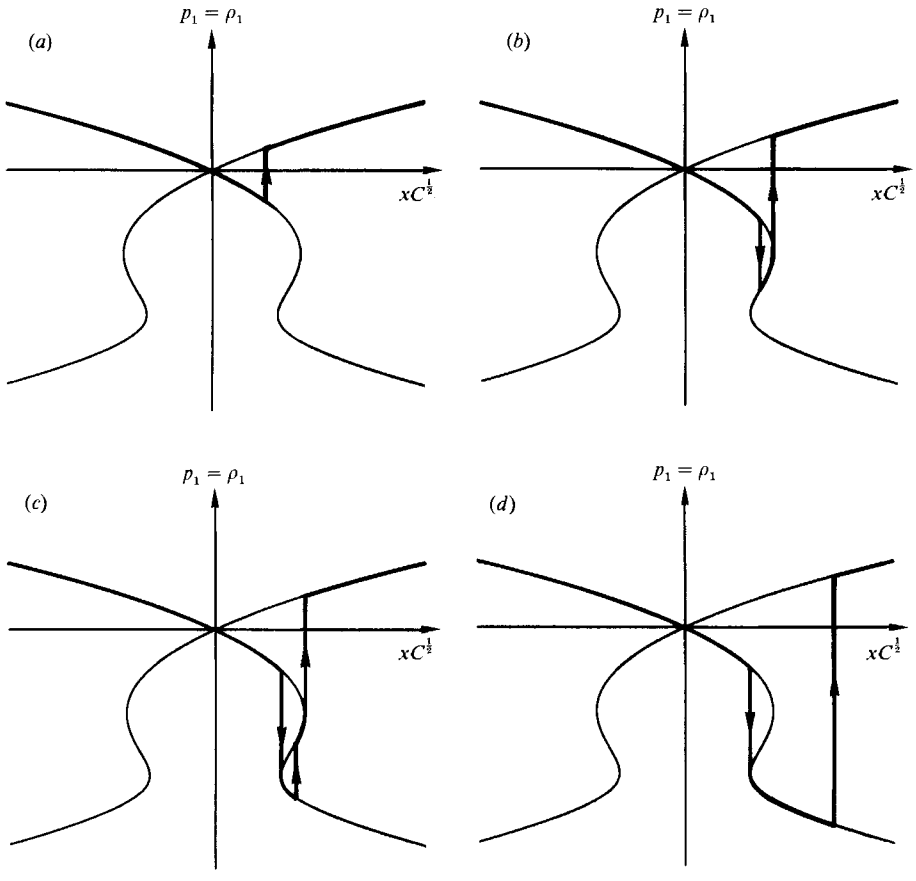

FIGURE 11. Laval nozzle: possible density distributions for $Q = Q_{\max}$ leading to subsonic flow far downstream; $\hat{\Gamma}_0 = 4.91$, $\hat{A}_0 = 15.80$, $\hat{N}_0 = 17.67$.

compression shock between the sonic expansion shock and the sonic compression shock. The requirement of increasing amplitude forces this shock to move downstream and it eventually merges with the sonic compression shock. The resulting single compression shock has $M \neq 1$ both upstream and downstream and its strength increases monotonically as it is shifted downstream. In this way one obtains the configuration shown in figure 11 (*d*) which, finally, can be extended to arbitrarily large shock amplitudes.

Investigation of the limiting case $\hat{\Gamma}_0 = \hat{A}_0^2/(3\hat{N}_0)$ leads to results which are qualitatively similar to those described above. It suffices to note, therefore, that the sonic expansion shock shown in figure 11 (*c*, *d*) has to be replaced by a double sonic shock at $x = 0$.

Interesting new flow patterns may form, however, if $\hat{A}_0^2/(3\hat{N}_0) > \hat{\Gamma}_0 > 0$. As pointed out earlier, the solution leading to a full subsonic–supersonic transition then includes a sonic expansion shock upstream of the throat, figure 8 (*e*). The requirement that the medium decelerates rather than accelerates downstream of the throat forces the second branch of the density distribution passing through the lower saddle point to come into play. The resulting solution is characterized by the presence of a sonic compression shock in the diverging part of the nozzle in addition to the sonic expansion shock upstream of the throat, figure 12 (*a*). By continuously increasing the

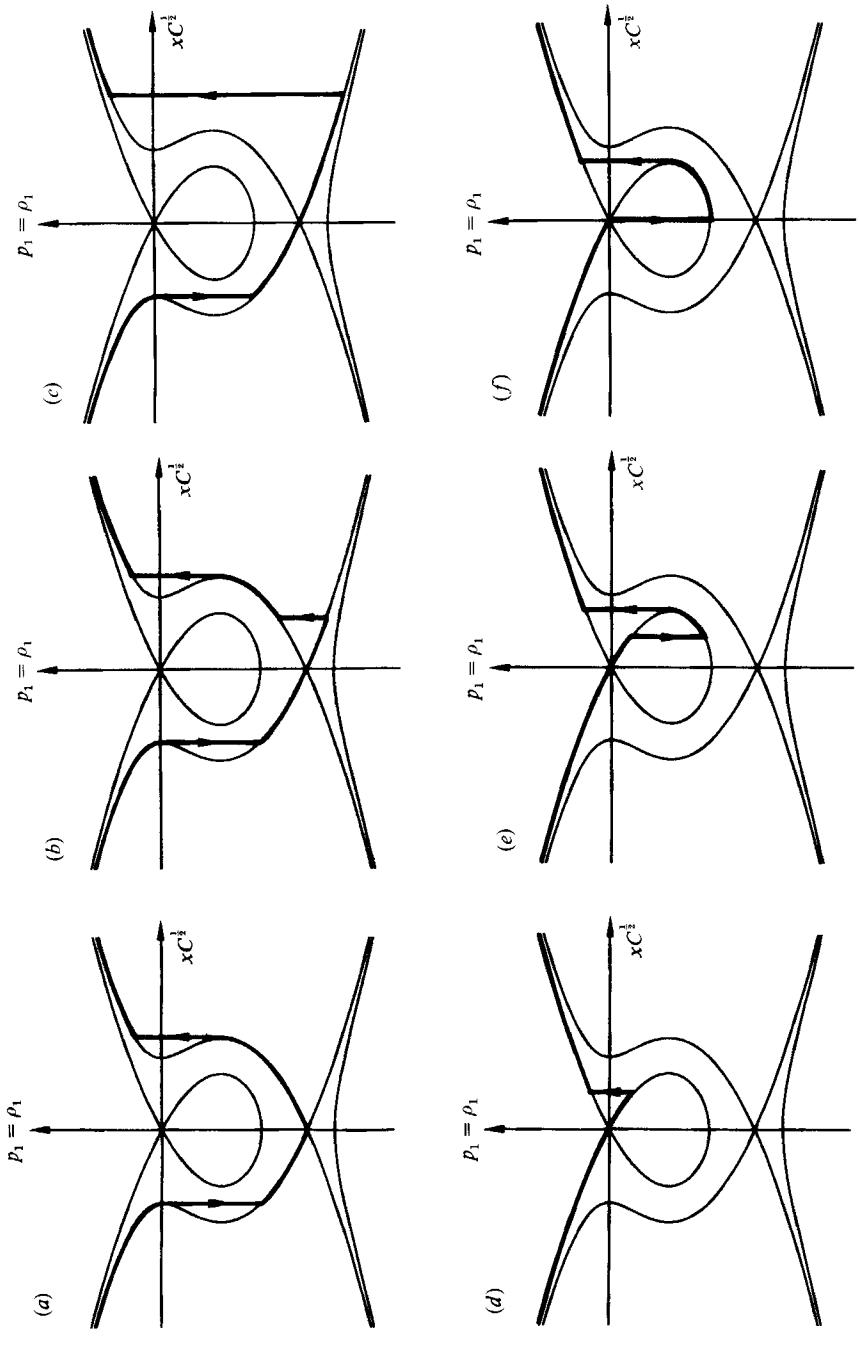

FIGURE 12. Laval nozzle: possible density distributions for $Q = Q_{\max}$ (a, b, c) and $Q = O$ (d, e, f) leading to subsonic flow far downstream; $\hat{\Gamma}_0 = 3.48$, $\hat{\Lambda}_0 = 14.03$, $\hat{N}_0 = 17.48$.

overall density jump occurring in the solution one obtains the flow configurations depicted in figure 12(*b*, *c*).

The results outlined so far hold if the perturbation mass flux Q assumes its maximum value $Q_{\max}$ thus yielding $M = 1$ at $x = 0$. Inspection of figure 8(*e*) shows that sonic conditions are reached at the throat also if the perturbation mass flux is reduced to $Q = 0$. The corresponding density distribution is, of course, of no relevance as far as a full subsonic–supersonic expansion of the medium is concerned. It can be used, however, to construct a second class of solutions describing flows which (eventually) decelerate in the diverging part of the nozzle after having been accelerated to sonic or even slightly supersonic speeds, figure 12(*d*, *e*). In contrast to the case $Q = Q_{\max}$ solutions with $Q = 0$ cannot be extended to arbitrarily large values of the overall shock strength. The limiting flow configuration shown in figure 12(*f*) is characterized by the presence of a sonic expansion shock at the throat $x = 0$.

The solutions summarized in figures 10, 11 and 12 are non-unique in the sense that families of them satisfy the same boundary conditions upstream of and far downstream of the throat $x = 0$ to leading order. In order to determine the relationship between the various possible shock configurations and the imposed conditions at the nozzle exit it would be necessary to account for the effects of the shock losses on the solution. It is tempting to expect that, for example, figure 11(*a–d*) describes the variation of the flow field caused by a slow quasi-steady reduction of the exit pressure. However, since the study of dense gases has already revealed a number of results which (guided by experience based on classical gasdynamics) must be regarded as grossly anti-intuitive, such a statement has to be considered with proper caution.

5. Shock structure

5.1. *Large Reynolds number approximation*

In general, the modified viscous transonic small-perturbation equation (3.15) has to be solved numerically. Here, we are mainly concerned with the thermoviscous structure of shocks in the limit of large Reynolds number, i.e. $\delta_0 \to 0$. For viscous terms to come into play, the shock thickness Δ has to be small: $\Delta = 0(\delta_0)$. As a consequence, it is convenient to introduce the stretched x-coordinate

$$\bar{x} = (x - x_s)/\delta_0, \tag{5.1}$$

where x_s denotes the location of the jump discontinuity as given by inviscid theory. Furthermore, since the cross-sectional area A varies only slightly across the shock profile, A_1 is written in the form

$$A_1 = A_1(x_s) + \delta_0 (\mathrm{d}A/\mathrm{d}x)(x_s)\,\bar{x} + o(\delta_0). \tag{5.2}$$

Substitution of (5.1) and (5.2) into (3.15) yields to leading order

$$\mathrm{d}\rho_1/\mathrm{d}\bar{x} = j_1^{\mathrm{inv}} - j_{1,s}^{\mathrm{inv}}. \tag{5.3}$$

Here, j_1^{inv} is the non-viscous part of the perturbation mass-flux density

$$j_1^{\mathrm{inv}} = -\hat{\Gamma}_0 \rho_1^2 - \tfrac{1}{3}\hat{A}_0 \rho_1^3 - \tfrac{1}{12}\hat{N}_0 \rho_1^4 \tag{5.4}$$

and the subscript s characterizes its value immediately before or after the shock.

5.2. *Asymptotic properties of shock profiles*

According to (5.3) the slope of the shock profile associated with a specific value ρ_1 is given by the difference between $j_1^{\mathrm{inv}}(\rho_1)$ and the mass-flux density $j_{1,s}^{\mathrm{inv}} = j_1^{\mathrm{inv}}(\rho_{1b}) = j_1^{\mathrm{inv}}(\rho_{1a})$ before and after the shock. As a result, some general features of shock profiles

can be inferred directly from the shape of the (j_1, ρ_1)-diagrams depicted in figure 9. For example, it is seen that three different cases have to be distinguished as far as the properties of the shock structure for $\rho_1 \to \rho_{1a}, \rho_1 \to \rho_{1b}$ are concerned.

If the Mach number M_e before or/and after the shock is different from 1 the local behaviour of $j_1^{inv} - j_{1,s}^{inv}$ for $|\rho_1 - \rho_{1e}| \ll 1$ can be approximated by

$$j_1^{inv} - j_{1,s}^{inv} \sim (j_1^{inv})'_e (\rho_1 - \rho_{1e}), \tag{5.5}$$

where a prime denotes differentiation with respect to ρ_1. Integrating (5.3) one obtains

$$\rho_1 - \rho_{1e} \sim C \exp\left[(j_1^{inv})'_e \bar{x}\right] \quad \text{as} \quad \bar{x} \to -\infty \quad \text{or/and} \quad \bar{x} \to +\infty. \tag{5.6}$$

Here C is an arbitrary constant.

In the case $(j_1^{inv})'_e = 0$, the shock under consideration is a sonic shock or a double sonic shock and (5.5) has to be replaced by

$$j_1^{inv} - j_{1,s}^{inv} \sim \tfrac{1}{2}(j_1^{inv})''_e (\rho_1 - \rho_{1e})^2. \tag{5.7}$$

As a consequence, the upstream or/and downstream asymptote of the shock profile is approached algebraically rather than exponentially

$$\rho_1 - \rho_{1e} \sim -\frac{2}{(j_1^{inv})''_e \bar{x}} \quad \text{as} \quad \bar{x} \to -\infty \quad \text{or/and} \quad \bar{x} \to \infty. \tag{5.8}$$

Finally, one has to consider sonic shocks having $(j_1^{inv})'_c = (j_1^{inv})''_c = 0$:

$$j_1^{inv} - j_{1,s}^{inv} \sim \tfrac{1}{6}(j_1^{inv})'''_e (\rho_1 - \rho_{1e})^3,$$

$$\rho_1 - \rho_{1e} \sim \pm \left[\frac{3}{|(j_1^{inv})'''_e \bar{x}|}\right]^{\frac{1}{3}} \quad \text{as} \quad \bar{x} \to -\infty \quad \text{or} \quad \bar{x} \to +\infty. \tag{5.9}$$

5.3. *Split shocks*

Inspection of figure 9 shows that shocks as typified by cases (i)–(iv), (vi) and (vii) lead to $j_1^{inv} - j_{1,s}^{inv}$ distributions which exhibit a single maximum or minimum. Consequently, the corresponding shock profiles qualitatively resemble classical Taylor shock profiles having a single inflexion point, figure 13(*a*). However, if the Rayleigh line $j_1^{inv} = j_{1,s}^{inv}$ falls below the minimum of the (j_1, ρ_1)-diagram (case (v) of figure 9) the resulting $j_1^{inv} - j_{1,s}^{inv}$ distribution will exhibit two maxima and a minimum, leading in turn to shock profiles with three inflexion points, figure 13(*b*). As the Rayleigh line approaches the minimum $j_1^{inv} = j_{1\min}$ of the j_1 versus ρ_1 curve from below, $j_{1,s}^{inv} - j_{1\min} \to 0-$, the slope of the shock profile at the middle inflexion point tends to zero and the overall density increase across the shock then is achieved, essentially, in two steps. Moreover, the density distributions associated with these steps which are separated by a pronounced plateau region, figure 13(*c*), differ only slightly from the limiting form of the shock profiles obtained for $j_{1,s}^{inv} - j_{1\min} \to 0+$, having sonic downstream and sonic upstream conditions, respectively. Owing to the slow algebraic decay law (5.8) holding for sonic shocks, the length of the plateau region increases without bound in the limit $j_{1,s}^{inv} - j_{1\min} \to 0-$ characterized by $M \to 1$ inside the plateau region, e.g. the shock splits. Physically, this means that the density jump corresponding to a position of the Rayleigh line touching the minimum of the (j_1, ρ_1)-diagram defines a lower bound for the strength of steady shocks which bridge the negative-Γ region. This ties in nicely with the third conclusion which follows immediately by inspection of the various possible $j_1^{inv} - j_{1,s}^{inv}$ distributions: steady

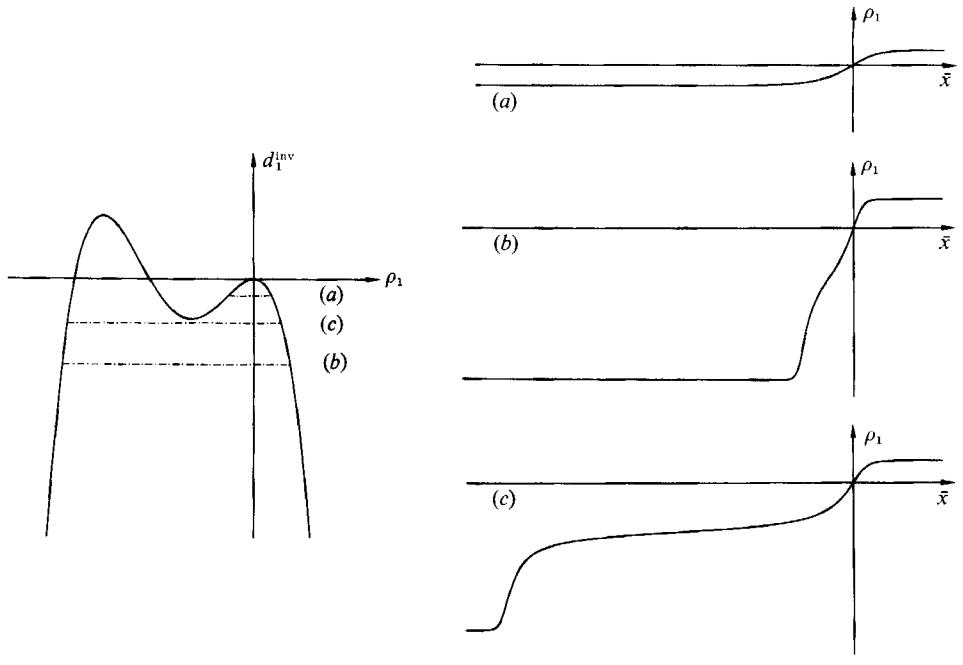

FIGURE 13. Different types of shock profiles ($\hat{\Gamma}_0 = 3.58$, $\hat{A}_0 = 14.22$, $\hat{N}_0 = 17.51$). (*a*) Profile with single inflexion point ; $j_{1,\rm s}^{\rm inv} = -0.2$. (*b*) Profile with three inflexion points: $j_{1,\rm s}^{\rm inv} = -1.0$. (*c*) Profile with pronounced plateau region: $j_{1,\rm s}^{\rm inv} = -0.48$.

shock profiles, e.g. solutions to (5.3), exist only if the Rayleigh line $j_1^{\rm inv} = j_{1,\rm s}^{\rm inv}$ does not cut the (j_1, ρ_1)-diagram at internal points of the interval $(\rho_{1\rm a}, \rho_{1\rm b})$.

The phenomenon of impending shock splitting was observed first in a different context by Cramer & Crickenberger (1991) who studied the dissipative structure of shock waves propagating in dense gases. By applying a weak shock approximation they were able to derive a single evolution equation and to obtain explicit solutions for shocks propagating with constant speed. The structure problem for shocks of this latter type is found to be completely equivalent to the structure problem for weak shocks in steady transonic flow formulated here. It therefore suffices to briefly summarize the analytical form of the solutions to (5.3). To this end the right-hand side of this equation is written as

$$j_1^{\rm inv} - j_{1,\rm s}^{\rm inv} = -\tfrac{1}{12}\hat{N}_0(\rho_1-\rho_{1\rm a})(\rho_1-\rho_{1\rm b})(\rho_1-\rho_1^+)(\rho_1-\rho_1^-), \tag{5.10}$$

where

$$\left.\begin{aligned} \rho_1^{\pm} &= \tfrac{1}{2}[-\alpha_1 \pm (\alpha_1^2 - 4\alpha_2)^{\frac{1}{2}}], \\ \alpha_1 = \rho_{1\rm a}+\rho_{1\rm b}+4\hat{A}_0/\hat{N}_0, &\quad \alpha_2 = \rho_{1\rm a}^2 + (\rho_{1\rm a}+\rho_{1\rm b})(\rho_{1\rm b}+4\hat{A}_0/\hat{N}_0) + 12\hat{\Gamma}_0/\hat{N}_0. \end{aligned}\right\} \tag{5.11}$$

Inspection of figure 9 shows that shocks of type (iii) are characterized by real values of $\rho_1^{\pm}$, while $\rho_1^{\pm}$ are complex conjugate for shocks of type (i) and (v). In the first case integration of (5.3) leads to

$$\begin{aligned} \tfrac{1}{12}\hat{N}_0\bar{x} = B_1 \ln\frac{\rho_{1\rm a}-\rho_1}{\rho_1-\rho_{1\rm b}} + B_2 \ln\left\{\frac{\rho_{1\rm a}-\rho_{1\rm b}}{\rho_1-\rho_{1\rm b}}\left[\frac{2(\rho_1-\rho_1^+)(\rho_1-\rho_1^-)}{(\rho_{1\rm a}+\rho_{1\rm b}-2\rho_1^+)(\rho_{1\rm a}+\rho_{1\rm b}-2\rho_1^-)}\right]^{\frac{1}{2}}\right\} \\ + \frac{1}{2B_5}(2B_3-\alpha_1 B_2)\ln\left\{\frac{\rho_1-\rho_1^+}{\rho_1-\rho_1^-}\left[\frac{\rho_{1\rm a}+\rho_{1\rm b}-2\rho_1^-}{\rho_{1\rm a}+\rho_{1\rm b}-2\rho_1^+}\right]^{\frac{1}{2}}\right\}. \end{aligned} \tag{5.12}$$

If $\rho_1^{\pm}$ are complex conjugate, however, one obtains

$$\tfrac{1}{12}\hat{N}_0\bar{x} = -B_1 \ln\left(\frac{\rho_{1a}-\rho_1}{\rho_1-\rho_{1b}}\right)+B_2 \ln\left\{\frac{\rho_{1a}-\rho_{1b}}{2(\rho_1-\rho_{1b})}\left[\frac{(2\rho_1+\alpha_1)^2+4B_4^2}{(\rho_{1a}+\rho_{1b}+\alpha_1)^2+4B_4^2}\right]^{\frac{1}{2}}\right\}$$
$$+\frac{1}{2B_4}(2B_3-\alpha_1 B_2)\left[\arctan\left(\frac{2\rho_1+\alpha_1}{2B_4}\right)-\arctan\left(\frac{\rho_{1a}+\rho_{1b}+\alpha_1}{2B_4}\right)\right]. \quad (5.13)$$

Here B_1, B_2, B_3, B_4 and B_5 are the quantities defined in Cramer & Crickenberger (1991) subject to the substitution u_1, u_2, $u^{\pm} \to \rho_{1b}$, ρ_{1a}, $\rho_1^{\pm}$.

Using (5.12) and (5.13) the form of the solution for shocks of type (ii), (iv), (vi) and (vii) can easily be deduced by carrying out appropriate limits in ρ_1^+, ρ_1^-.

To conclude this section we note that the pressure, temperature, velocity, entropy and Mach number distributions across weak steady transonic shocks can be determined immediately from the density profiles discussed so far by applying (3.18) and (3.13) if desired.

6. Conclusions

The main objective of the present study was to deepen our understanding of transonic nozzle flows in the dense gas regime, which are expected to play an important role in new engineering applications of working fluids having large specific heats. The investigations are based on the standard Navier–Stokes equations supplemented with non-standard constitutive relationships.

Adopting the assumption of quasi-one-dimensional flow, a perturbation analysis is carried out which leads to a novel form of the viscous transonic small-perturbation equation. Solutions to the non-dissipative version of this equation indicate that classical convergent–divergent nozzles are not suitable to generate shock-free flows if the medium is taken from one side of the $\Gamma > 0$ region to the other side as it accelerates from subsonic to supersonic speeds. In order to avoid the occurrence of shocks nozzles of rather unconventional shape with two throats are found to be necessary.

Investigation of the jump relationships for weak shocks shows that the condition $[s] \geqslant 0$ following from the second law of thermodynamics is not sufficient to rule out inadmissible discontinuities, e.g. shocks for which a dissipative structure does not exist. Admissible shocks must satisfy the additional requirement that the Rayleigh line does not cut the isentrope connecting the upstream and downstream state in internal points. Shocks which satisfy this admissibility criterion may occur in the form of compression/expansion shocks leading from supersonic to subsonic speeds or in the form of sonic/double sonic shocks having sonic upstream or/and downstream conditions. Furthermore, analysis of the shock structure problem indicates that compression shocks which bridge the whole $\Gamma < 0$ region may exhibit density (pressure, temperature) profiles with three inflexion points rather than a single inflexion point if the shock strength S exceeds a critical value S_c. As the shock strength decreases and approaches the critical value the overall density increase is achieved, essentially, in two (almost independent) steps. The density profile then comprises two (almost) classical density distributions having one inflexion point each which are separated by a pronounced plateau region. In the limit $S - S_c \to 0+$ the length of the plateau region increases without bound and the shock splits. A similar phenomenon was observed in a different context by Cramer & Crickenberger (1991) who studied the dissipative structure of finite-amplitude shock waves in dense gases.

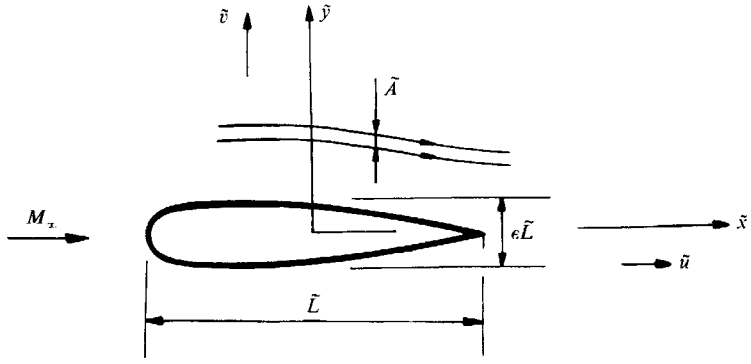

FIGURE 14. Transonic flow past slender airfoil.

6.1. *Modified viscous transonic small-perturbation equation for external flows*

Although the phenomena presented in this study are of interest in their own right, it is felt that they can have a broader relevance. For example, the results derived here for transonic internal flows can be used immediately to infer the proper form of the governing equations for transonic external flows. To this end we consider the flow past a slender airfoil at a small angle of attack, figure 14. The subscript ∞ is used to denote the values of the various field quantities evaluated at free-stream conditions.

First, the flow inside a narrow stream tube formed by two neighbouring streamlines is certainly quasi-one-dimensional and can thus be modelled mathematically by the equations for internal flows. Second, since the inclination of the streamlines with respect to the free-stream direction is small, the changes of the cross-sectional area A with distance x is proportional to the variation of the lateral velocity component $\bar{v}$ in the y-direction:

$$\frac{1}{A}\frac{\mathrm{d}A}{\mathrm{d}x} \sim \frac{\partial \bar{v}}{\partial y}, \tag{6.1}$$

$$x = \tilde{x}/\tilde{L}, \quad y = \tilde{y}/\tilde{L}, \quad \bar{v} = \tilde{v}/\tilde{u}_\infty. \tag{6.2}$$

Third, since the flow is transonic the negative density perturbations and the perturbations of the streamwise velocity component $\bar{u}$ agree to a first approximation:

$$\bar{u} = (\tilde{u}-\tilde{u}_\infty)/\tilde{u}_\infty \sim -(\tilde{\rho}-\tilde{\rho}_\infty)/\tilde{\rho}_\infty = -\bar{\rho}. \tag{6.3}$$

Fourth, in studies dealing with external flows it is convenient to non-dimensionalize the various field quantities with their free-stream values rather than with the values corresponding to critical flow conditions. As a consequence, the expression for the perturbation mass flux $\bar{j} = (\tilde{\rho}\tilde{u}-\tilde{\rho}_\infty\tilde{u}_\infty)/\tilde{\rho}_\infty\tilde{u}_\infty$ contains the additional term $(1-M_\infty^2)\,\bar{u}$:

$$\bar{j} = (1-M_\infty^2)\,\bar{u} - \Gamma_\infty\,\bar{u}^2 + \tfrac{1}{3}A_\infty\,\bar{u}^3 - \tfrac{1}{12}N_\infty\,\bar{u}^4 + \bar{\delta}_\infty\,\partial\bar{u}/\partial x. \tag{6.4}$$

Substitution of (6.1) into the linearized form of the continuity equation for slender streamtubes assuming irrotational flow leads to

$$\frac{\partial \bar{j}}{\partial x} + \frac{\partial \bar{v}}{\partial y} = 0, \quad \frac{\partial \bar{u}}{\partial y} - \frac{\partial \bar{v}}{\partial x} = 0. \tag{6.5}$$

Introducing the perturbation velocity potential $\bar{u} = \phi_x, \bar{v} = \phi_y$ this result can be written in the equivalent form

$$(1-M_\infty^2 - 2\Gamma_\infty\,\phi_x + A_\infty\,\phi_x^2 - \tfrac{1}{3}N_\infty\,\phi_x^3)\,\phi_{xx} + \phi_{yy} = -\bar{\delta}_\infty\,\phi_{xxx}. \tag{6.6}$$

Working medium	$\lvert M_\infty - 1\rvert$	c_p
Perfect gas: $\Gamma_0 = O(1)$	$O(\epsilon^{\frac{2}{3}})$	$O(\epsilon^{\frac{2}{3}})$
BZT fluid: $\Gamma_0 = O(\epsilon^{\frac{1}{2}})$	$O(\epsilon)$	$O(\epsilon^{\frac{1}{2}})$
BZT fluid: $\Gamma_0 = O(\epsilon^{\frac{4}{5}})$	$O(\epsilon^{\frac{6}{5}})$	$O(\epsilon^{\frac{2}{5}})$

TABLE 1. Extent of the Mach number range and magnitude of pressure disturbances for transonic flow of perfect gases and BZT-fluids.

Equation (6.6) represents a modified version of the viscous transonic small-perturbation equation for perfect gases $\Lambda_\infty = N_\infty = 0$ derived first by Liepmann, Ashkenas & Cole (1950). In the limit $N_\infty = 0$, $\delta_\infty = 0$ it reduces to the equation obtained by Cramer (1991*b*) which is valid near one of the high- or low-pressure zeros of the fundamental derivative. As in this case, the incorporation of dense gas effects into the theory of transonic external flows is found to lead to a significant increase/decrease of the lower/upper critical Mach number, e.g. to a significant reduction of the nonlinear transonic flow regime.

By definition the lower critical Mach number M_{crit} is the free-stream Mach number at which the local Mach number first becomes sonic for a given airfoil shape. If M_∞ is sufficiently smaller than M_{crit} linear theory applies. According to this theory

$$\bar{u} = O(\epsilon/(1-M_\infty^2)^{\frac{1}{2}}), \tag{6.7}$$

where $\epsilon \ll 1$ characterizes the thickness ratio of the airfoil. Nonlinear effects, however, have to be taken into account if the changes of

$$1-M^2 = 1-M_\infty^2 - 2\Gamma_\infty \bar{u} + \Lambda_\infty \bar{u}^2 - \tfrac{1}{3}N_\infty \bar{u}^3 \tag{6.8}$$

resulting from these velocity disturbances are comparable in magnitude with $1-M_\infty^2$, in other words if $1-M_\infty^2$ and $\Gamma_\infty \bar{u}$ are the same order of magnitude. The way in which the free-stream value of the fundamental derivative influences the extent of the transonic flow regime is, therefore, quite obvious: decreasing values of Γ_∞ must be balanced by decreasing values of $1-M_\infty^2$, e.g. by increasing values of M_{crit}. Using the Prandtl–Glauert relationship (6.7) and expression (6.8) for the local Mach number distribution the magnitude of this and related effects can easily be estimated analytically. As in the treatment of internal flows two different cases have to be distinguished. In the first case, studied recently by Cramer (1991*a*), and Cramer & Tarkenton (1992), sonic conditions are reached near one of the high- or low-pressure zeros of Γ. Accordingly, the value of the fundamental derivative in the unperturbed flow is of the order of a characteristic velocity disturbance: $\Gamma_\infty = O(\bar{u})$. Furthermore, $\Lambda_\infty = O(1)$ and the terms of (6.6), (6.8) proportional to N_∞ can be neglected to leading order. In the second case which is of interest here, the reference state is in the neighbourhood of the thermodynamic state having $\Gamma = 0, \partial\Gamma/\partial\rho|_s = 0$. Consequently, we require $\Gamma_\infty = O(\bar{u}^2)$, $\Lambda_\infty = O(\bar{u})$ and $N_\infty = O(1)$.

The results summarized in table 1 show the expected narrowing of the nonlinear transonic flow regime occurring in dense gases. According to the Prandtl–Glauert relationship (6.7) the associated increase of the lower critical Mach number leads to an increase of the velocity and pressure disturbance level in the flow field. As a consequence, dense gases may generate substantially higher lift than perfect gases with no increase of the wave drag as long as the occurrence of shocks is avoided. Once shocks form, however, the resulting increase of the drag coefficient is more severe than in the classical case.

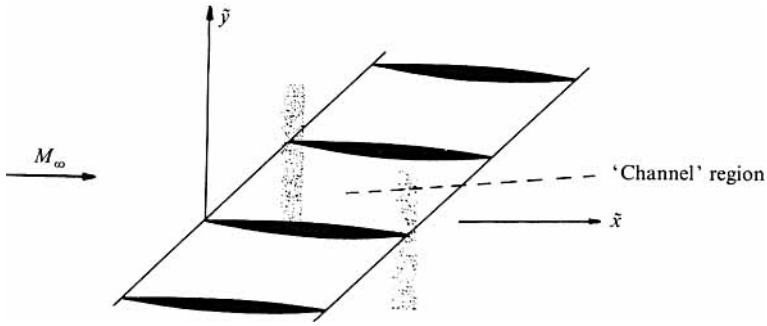

FIGURE 15. Schematic of lightly loaded transonic cascade.

6.2. *Lightly loaded transonic cascades*

The above considerations indicate that dense gases may prove beneficial as working fluids in turbomachines. In this connection, the design of transonic cascades represents an important and difficult task. The complete version of the small-perturbation equation (6.6) applies to the case that the spacing between the blades is much larger than the chord length, this ratio being of the order $1/(1-M_{\mathrm{crit}}^2)^{\frac{1}{2}}$. In many cases of practical importance, however, the blade spacing is typically comparable with the chord length and the calculations can then be simplified considerably using the method of matched asymptotic expansions as pointed out first by Messiter & Adamson (1981) in a study of classical transonic flow. The most interesting implication is that a portion of the flow between any two adjacent airfoils is described in a first approximation as a one-dimensional internal flow. For a certain combination of parameters (thickness ratio, camber, angle of attack) presently under investigation this flow is governed by nonlinear equations of the form as derived in §4, figure 15. The flow ahead and downstream of the channel is purely subsonic or supersonic, and the equations are found to be two-dimensional but linear. Since the solutions holding in the channel region and the regions before and after the channel do not match, additional solutions in thin strips centred at the leading and trailing edges are also needed. In this way the overall flow problem is divided into a number of simpler problems which can be solved analytically. Preliminary considerations confirm the trends observed for single airfoils that dense gas effects may be exploited to increase the lift force acting on the blades with no increase of the drag if the formation of shocks is avoided.

The author wants to thank Dr Ph. Gittler, Dipl.-Ing. G. Lindner and Dipl.-Ing. J. Maklad for their assistance with the numerical computations.

REFERENCES

BETHE, H. A. 1942 The theory of shock waves for an arbitrary equation of state. *Office Sci. Res. Dev. Rep.* 545.

CHANDRASEKAR, D. & PRASAD, P. 1991 Transonic flow of a fluid with positive and negative nonlinearity through a nozzle. *Phys. Fluids* A **3**, 427–438.

CRAMER, M. S. 1989 Negative nonlinearity in selected fluorocarbons. *Phys. Fluids* A **1**, 1894–1897.

CRAMER, M. S. 1991*a* Transonic flows of BZT fluids. In *Proc. 13th World Congr. on Computation and Applied Mathematics (IMACS 91)*, pp. 570–571.

CRAMER, M. S. 1991*b* Nonclassical dynamics of classical gases. In *Nonlinear Waves in Real Fluids* (ed. A. Kluwick), pp. 91–145. Springer.

CRAMER, M. S. & CRICKENBERGER, A. B. 1991 The dissipative structure of shock waves in dense gases. *J. Fluid Mech.* **223**, 325–355.

CRAMER, M. S. & KLUWICK, A. 1984 On the propagation of waves exhibiting both positive and negative nonlinearity. *J. Fluid Mech.* **142**, 9–37.

CRAMER, M. S. & TARKENTON, G. M. 1992 Transonic flows of Bethe–Zel'dovich–Thompson fluids. *J. Fluid Mech.* **240**, 197–228.

KLUWICK, A. 1991 Small-amplitude finite-rate waves in fluids having both positive and negative nonlinearity. In *Nonlinear Waves in Real Fluids* (ed. A. Kluwick), pp. 1–43. Springer.

LAMBRAKIS, K. C. & THOMPSON, P. A. 1972 Existence of real fluids with a negative fundamental derivative *Γ*. *Phys. Fluids* **5**, 933–935.

LIEPMANN, H. W., ASHKENAS, H. I. & COLE, J. D. 1950 Experiments in transonic flow. *Wright Air Dev. Cent. Tech. Rep.* 5667.

MARTIN, J. J. & HOU, Y. C. 1955 Development of an equation of state for gases. *AIChE J.* **1**, 142–151.

MESSITER, A. F. & ADAMSON, T. C. 1981 Transonic small disturbance theory for lightly loaded cascades. *AIAA J.* **19**, 1047–1054.

OLEINIK, O. A. 1959 Uniqueness and stability of the generalized solution of the Cauchy problem for a quasilinear equation. *Usp. Mat. Nauk* **14**, 165–170. (English Transl.) *Am. Math. Soc. Transl. Ser* 2, **33**, 285–290.

THOMPSON, P. A. 1971 A fundamental derivative in gasdynamics. *Phys. Fluids* **14**, 1843–1849.

THOMPSON, P. A. & LAMBRAKIS, K. C. 1973 Negative shock waves. *J. Fluid Mech.* **60**, 187–207.

ZEL'DOVICH, YA. B. 1946 On the possibility of rarefaction shock waves. *Zh. Eksp. Teor. Fiz.* **4**, 363–364.